AGS PREINJECTOR BEAM EMITTANCE AREA AND EMITTANCE AREA DENSITY DISTRIBUTION MEASUREMENTS

A. van Steenbergen
Brookhaven National Laboratory

Early efforts to raise the linac proton current intensity by increasing the preinjector output current showed that the linac output current did not increase linearly with the preinjector current. Especially at the highest preinjector currents obtained (≅ 90 ma total pulsed current), beam losses could be of the order of 50% compared with theoretical values; that is, values calculated on the basis of rf capture and proton percentage only.

Preliminary investigations showed that large preinjector beam emittance values, coupled with a limited linac transverse phase space acceptance, could be responsible for the beam losses to a great extent. Measurements of the preinjector beam emittance area were made with the P.I.G. source*, whereby preinjector currents of up to 30 ma total currents could be obtained and with the duoplasmatron source*, whereby preinjector output currents of up to 90 ma were observed.

Preliminary investigations with the duoplasmatron ion source, using a low voltage test bench (up to 100 kv), indicated that this source is capable of producing substantial higher particle beam intensities than the P.I.G. source. With the same focusing system in the preinjector low energy end as is presently in use with the P.I.G. source, higher beam

*"Linac Conference Report", 1961, BNL, IA AvS-1, p.91

intensities could result in larger beam emittance area values. First, because the higher beam intensities could be obtained from a larger plasma boundary area resulting in a larger emittance area value observed adjacent to the ion source. Second, the influence of space charge forces and also a resultant larger filling of lens apertures with consequent increased aberrations could affect the emittance area* .

Because ion source parameters and extraction region geometries may have a pronounced influence on beam emittance, a systematic study was undertaken to measure beam emittance area, phase space density distribution, and maximum obtainable beam intensity at 750 kev as a function of various duoplasmatron parameters and extraction geometries.

Experimental Arrangement

The pertinent components of the AGS preinjector are shown in Fig. 1. To accommodate emittance measurements, the normal arrangement for beam steering and bunching was removed and extra slit arrangements plus Faraday cups were installed. This is shown in Fig. 2. All slits were driven by threaded shafts which were coupled to mechanical counters, such that slit positions could be set and reproduced to within 0.1 mm, as long as a consistent sense of rotation was adopted. All slits, except the first vertical slit, were 1/32 inches wide ($\cong$3/4 mm) in order to permit small enough sampling of the beam. The beam diameter was usually of the order of 20 to 30 mm at the location of the first slits. With a distance of approximately 54 inches between slits, an angular sampling unit of 1.1^5 mrad was used throughout the measurements. The first vertical slit is made in a thin sheet of metal which could be rotated into the beam. For small adjustments of its angular position around 45^o with respect to the propogation direction of the beam, its slit width perpendicular to the beam was essentially unchanged and approximately 1 mm wide.

*A. van Steenbergen, Internal Report, BNL, AvS-2 (Appendix)

In order to obtain correct values of the emittance area $F(y,\alpha_y)_{x=o}$ and the density distribution in phase space, it is essential that the vertical slits be centered in the beam. This proved to be simpler than anticipated. At first, centering of both vertical slits and determination of zero position of the horizontal slits was done by measuring the current through into the Faraday cup. For a more or less homogeneous beam, slight variations around the zero positions do not result in pronounced changes in Faraday cup current. Subsequently, it was noticed that with two crossed slits intercepting the beam, observation of the image on the quartz plate in the large Faraday cup provides a far more sensitive means for centering the slits. This is because misalignments of the vertical slits or first horizontal slit results in pronounced asymmetries of the image pattern. By observing this, centering of the slits and determination of the zero position could be obtained within a maximum error of the order of 0.5 mm (5 digits of the slit drive mechanism).

Transverse Phase Space Area and Density Distribution Determination

Consider a particle beam propagated along the z-axis as illustrated in Fig. 3a. To obtain the transverse phase space representation $F(y,p_y)_{x=o}$ a sample of the beam, defined by the crossed slits 1 is being scanned by a horizontal slit 2 plus Faraday cup, whereby its horizontal extent is being limited by the second vertical slit. A resultant beam intensity distribution is illustrated in Fig. 3b. The angular extent of the beam sample under consideration in the $(Y\text{-}Z)_{x=o}$ plane is now obtained from the zero intensity points P and Q. The same procedure is followed for different positions of the first horizontal slit resulting in the beam emittance boundary $F(y,\alpha_y)_t = F(y,p_y/p_z)_t$ as given in Fig. 3c. (Note area $F(y,p_y)_{x=o}$ = invariant.)

Omitting in this case the vertical defining slits would for a "more or less well behaved" beam give the same result. This is because for $y=y_1$, $x=o$, the angular divergence is generally larger than for any $y=y_1$, $x\neq o$ sample of the beam. A hypothetical intensity distribution of a corresponding beam sample without vertical slits is given in Fig. 3d.

To obtain now a density distribution within the emittance area $F(y,\alpha_y)_t$ one obtains a new angular extent P_f, Q_f, found by using cut-off values determined by an arbitrary fraction of the peak intensity, as shown in Fig. 3b. By integrating now the beam intensity defined by the so limited curves and that enclosed by the original curves one obtains that fraction of the total beam which is represented in the new $F(y,\alpha_y)_f$ emittance boundary. In this case the omission of the defining vertical slits would yield different values for the calculated fraction of the total beam represented by $F(y,\alpha_y)_f$. This is because in the latter case mixed components (say $y=y_1$, $x\neq o$) are taken into account by integrating the intensity distribution curves. Consequently, an emittance area $F(y,\alpha_y)$ with density distribution contours should be identified with the fact that it is obtained with $x=o$ components only or with all $-\infty<x<+\infty$ components.

The foregoing procedure is further illustrated by a detailed example of actual measurements. This is the case of an emittance area $F(y,\alpha_y)_{x=o}$ density distribution determination of a 750 kev, 80 ma, beam from the preinjector. Intensity distributions for $y_1=o$ to $y_1=+\infty$ (half beam diameter) are given in Fig. 4. Because of symmetry with respect to the $y=o$ plane, this is sufficient to plot an emittance boundary. Initial measurements considering all y_1 values confirmed the symmetry. Taking now the maximum intensity of the $y_1=o$ distribution as a 100% value, all zero intensity points (P_t,Q_t; Fig. 3b) were determined at 1% of this value.

Again, earlier observations and calculations showed that the emittance area thus obtained represents about 99% of the total beam. The intensity distributions are now cut off at 10%, 20%, and 40% of the y_1=o maximum intensity value, as shown in Fig. 4. Let A_{ti} represent the integrated distribution for y_1=i within the 1% cut-off values and A_{fi} the corresponding values within say 20% values. Then the total current represented by $F(y,\alpha_y)_t$ is

$$I_t=A_o+p\left(\frac{A_o+A_1}{2}\right)+A_1+\ldots+p\left(\frac{A_o+A_{-1}}{2}\right)+A_{-1}+\ldots=2(p+1)\left\{\frac{A_{to}}{2}+\sum_1^\infty A_{ti}\right\}$$

where $p=\Delta y_1/\delta$, δ=slit width and taking $A_i=A_{-i}$. Similarly, the fractional current I_f represented by $F(y,\alpha_y)_f$ is

$$I_f=2(p+1)\left\{\frac{A_{fo}}{2}+\sum_1^\infty A_{fi}\right\}$$

The resultant emittance boundaries are shown in Fig. 5. The triangles, crosses, and circles indicate boundaries obtained from a complete repeat measurement, with a time lapse of one day. Good reproducibility is indicated by comparing this with the continuous curves.

Typically, in this particular case the following values are obtained: 750 kev, 80 ma total beam.

Intensity distribution cut-off values	1	10	20	40%
Fractional beam intensity (I_f/I_t). 100%	99	93	85	72%
Absolute beam intensity	79	74	68	57 ma
Represented by the corresponding emittance area $F(y,\alpha_y)_{x=o}$	413	214	147	90 mm-mrad

Experimental Results

The pertinent section of the duoplasmatron source with extraction electrode is shown in Fig. 6 and Fig. 7. The plasma normally extends into the aperture cup and its boundary location and extent is determined by plasma density (ion source electrical parameters), cup geometry, magnetic flux path and extraction field shape and magnitude. For a certain current output the beam emittance area will be affected by plasma boundary shape and extent and so indirectly by the above mentioned parameters. Also the size of the expanding beam cone in this region will affect the beam diameter in the optical system.

This reasoning led to a choice of parameters for which an emittance area determination would be interesting. Of necessity, a limit is imposed by time on all the numerous combinations available. Also several parameters were investigated previously on the ion source test bench. The magnetic flux path is such that optimum ion source stability and maximum current output is obtained by choice of the diameter of bore in the mild steel anode. This also determines the plasma expansion cup diameter. Also the distance between intermediate electrode and anode is fixed because of optimum proton percentage in the total beam, also previously investigated.

Referring back now to Fig. 6 and Fig. 7, emittance plots and emittance area density distributions were obtained for the combination of parameters shown in Table 1.

In general, being interested in high current output, emittance area measurements were done for maximum 750 kev current output obtainable with the pertinent set of geometrical parameters and optimum combination of electrical parameters, i.e., discharge current, magnet current, etc.

Table 1

		Extraction Region Geometrical Parameters						Duoplasmatron Parameters			Preinjector Optical Parameters						
Comb. of Param-eters	Emit-tance Plot Fig.	d in. $x10^{-3}$	T in. $x10^{-3}$	L in. $x10^{-3}$	G in. $x10^{-3}$	D in.	S in.	Anode Volt. v.	Magn Curr amp.	Dischg Curr amp.	Extrac. kv	F_1 kv	F_2 kv	High Lens +kv	Energy Volt. -kv	Output Current I_{tot} ma	Area $F(y,\alpha_y)_{x=o}$ for 90% of I_{tot} mm-mrad
I	8	20	5	120	200	0.5	3.6	300	2.2	29	40	70	22	15	15	36	240
II	9	20	5	120	200	0.5	3.6	280	2.4	25	40	70	22	15	15	33	210
III	10	20	5	120	160	0.19	3.6	160	3.0	15	35	60	22	10	10	42	100
IV	11	20	5	120	160	0.19	3.6	160	3.0	15	35	60	22	5	5	40	95
V	12	20	5	120	160	0.19	3.6	160	3.0	15	45	70	22	10	10	55	200
VI	13	20	20	105	160	0.19	3.6	300	2.8	30	40	65	22	13	13	40	295
VII	14	20	20	105	200	0.5	3.6	150	3.3	15	43	70	22	13	13	34	150
VIII		20	5	0	200	0.5	3.6	200	3.0	16	45	65	22	15	15	5	
IX		50	20	0	55	0.19	3.6	250	2.0	20	40	70	22	12	12	38	
X	15	20	15	55	115	0.19	3.6	170	4.0	15	43	72	22	15	15	30	135
XI	16	20	5	120	115	0.19	3.6	200	3.4	17	42	72	22	15	15	68	195
XII	17	20	5	120	115	0.25	3.6	200	3.2	16	43	72	22	16	16	62	260
XIII		20	5	120	115	0.19	4.4	200	2.0	18	45	70	22	10	10	50	
XIV		20	5	120	115	0.19	2.8	200	2.8	16	35	68	22	14	14	72	
XV	18	25	5	120	115	0.19	2.8	160	2.7	15	35	70	22	12	12	80	190
XVI	19	25	5	120	115	0.19	2.8	160	2.7	12	35	70	22	12	12	40	150

A few cases are mentioned in Table 1 whereby no emittance area measurements were done because the maximum output current was the only result of interest in that case. These are mentioned, however, to illustrate the total beam output as a function of geometry.

The measured emittance area plots are shown in Figs. 8 through 19. Each one is denoted with a Roman numeral which refers back to the combination of parameters given in Table 1. The resultant values are tabulated in Table 2. From this, in order to compare results for the various combinations of parameters, emittance area values are obtained representing 80% and 90%, respectively, of the total beam. This is listed in Table 3. This was done by interpolation of graphs of emittance area value versus enclosed current for each case. An example of this is shown in Fig. 20. These curves are typical for all cases and illustrate the fact that the beam density is relatively low in the outer fringes of the emittance areas. Generally, at a sacrifice of only 10% of the total beam intensity, an emittance area value is obtained of approximately half of that representing the total beam intensity.

For ease of interpretation, the emittance area values representing 90% of I_{tot}, given in Table 3, are indicated in Table 1.

It proved interesting now to plot, for all combinations investigated, independent of geometry and parameters, the emittance area values given in Table 3 versus the absolute values of current represented by these areas. The results are shown in Figs. 21a and 21b and indicated by Roman numerals. These refer to the corresponding combination of parameters given in Table 1. The two circles in Fig. 21b indicate the corresponding results obtained with the P.I.G. source as ion source in the preinjector. (The triangles shown in Figs. 21a and 21b are not pertinent to the present discussion.) A straight

Table 2

Comb. of Para-meters	Emittance Plot	I_{tot}	Area $F(y,\alpha_y)_{x=o}$	Representing % of I_{tot}	Area $F(y,\alpha_y)_{x=o}$	Representing % of I_{tot}	Area $F(y,\alpha_y)_{x=o}$	Representing % of I_{tot}	Area $F(y,\alpha_y)_{x=o}$	Representing % of I_{tot}
	Fig.	ma	mm-mrad	%	mm-mrad	%	mm-mrad	%	mm-mrad	%
I	8	36	461	98	232	89	172	80		
II	9	33	356	98	247	93	175	82		
III	10	42	228	99	135	95	100	90		
IV	11	40	197	99	117	94	81	85		
V	12	55	430	99	264	96	189	88	128	75
VI	13	40	561	99	294	90	194	81		
VII	14	34	262	99	117	86	76	76		
X	15	30	322	99	114	88	74	79		
XI	16	68	403	99	206	93	169	84	112	69
XII	17	62	456	99	255	90	170	77	109	61
XV	18	80	413	99	214	93	147	85	90	72
XVI	19	40	260	99	158	91	97	79	50	58

Table 3

Comb. of Para-meters	Emittance Plot	I_{tot}	Area $F(y,\alpha_y)_{x=o}$ for 90% of I_{tot}	Area $F(y,\alpha_y)_{x=o}$ for 80% of I_{tot}	$\frac{I_f\ (90\%)}{\text{Area } F(y,\alpha_y)_{x=o} \text{ for 90\% of } I_{tot}}$ $(=\rho_1)$	$\frac{I_f\ (80\%)}{\text{Area } F(y,\alpha_y)_{x=o} \text{ for 80\% of } I_{tot}}$ $(=\rho_2)$	R = ρ_1/ρ_2	Acceptable Current for Area $F(y,\alpha_y)_{x=o}$ =150 mm-mrad	
								% of I_{tot}	Actual Current
	Fig.	ma	mm-mrad	mm-mrad	ma/ mm-mrad	ma/ mm-mrad		%	ma
I	8	36	240	172	$1.3^5 \times 10^{-1}$	$1.6^5 \times 10^{-1}$	1.2^5	70	25
II	9	33	210	170	1.3^5	1.5^5	1.1^5	70	23
III	10	42	100	80	3.8	4.2	1.1	96	40
IV	11	40	95	70	3.8	4.5^5	1.2	97	39
V	12	55	200	145	2.5	3.0^5	1.2	80	44
VI	13	40	295	185	1.2^5	1.7	1.4	70	28
VII	14	34	150	85	2.0^5	3.2	1.5^5	91	31
X	15	30	135	75	2.0	3.2	1.6	90	27
XI	16	68	195	135	3.1	4.0	1.3	80	55
XII	17	62	260	170	2.1^5	2.9	1.3^5	73	46
XV	18	80	190	120	3.8	5.3^5	1.4	86	69
XVI	19	40	150	100	2.4	3.2	1.3	90	36

line is drawn to indicate a trend of emittance area value versus pre-injector output current. It should be stated again that all points refer to various combinations of parameters and no expectation exists that these values could be represented by a straight line. Only in the case of Combinations XV and XVI were all parameters nearly identical. There the output current was decreased by lowering the ion source pressure to 60 microns. For all Combinations I through XV, the source pressure was kept constant at 200 microns.

Fig. 21 indicates that with the present optical arrangement in the preinjector an increase in output current by a factor of two results in an increase of the corresponding emittance area by approximately the same factor.

Analysis of the Results

Referring again to Fig. 21, an examination of the results shows that in three cases emittance areas were obtained having markedly higher values, at currents of approximately 30 ma, than the dashed line indicates. This is the case for Combinations I, II and VI. Comparing parameters for the various combinations the different behavior seems to be connected with the duoplasmatron parameters, namely that for the three cases mentioned, the anode voltage was substantially higher than for all other combinations (see Table 1). The reason for using higher anode voltage values at times is connected with the state of the emission coated filament used in the duoplasmatron source. Using a freshly coated filament, best performance was always obtained with the ion source running at a relatively low anode voltage. Increasing in this case the anode voltage led to higher discharge currents and plasma densities, with consequent increase in output current. This resulted then in breakdown in the extraction region. The optical system proved to be the limiting factor on maximum output current in this case. With a filament which was used for some

time and manifestly inferior, the same maximum output currents, limited similarly, could only be obtained with pronounced higher anode voltages. As indicated, in these cases, substantial larger emittance area values were obtained. No sensible explanation is available as yet why this should be so. It is difficult to imagine a mechanism whereby in the duoplasmatron source the plasma boundary shape and/or the thermal energies of the expanded plasma (at near zero potential) in the aperture cup should be affected by the state of the secondary plasma within the intermediate electrode of this source.

Before considering all results in general, each combination of parameters will be reviewed briefly.

Comb. I, II. The relatively large emittance area values obtained here are assumed to be connected with a distinct mode of operation of the duoplasmatron source, as indicated above. The consideration that the results might be due to the extraction geometry, whereby in these cases the extraction electrode had a 1/2 inch diameter aperture, resulting in a reduced focusing action in the extraction region is opposed by the emittance area results of Combination VII where approximately the same output current was obtained with almost identical geometrical and optical parameters.

Comb. III, IV, V. These measurements were done with identical geometrical and duoplasmatron parameters. In cases III and IV, the optical parameters were also nearly the same. As expected, the emittance area values (Table 3) are approximately equal; the difference should be taken as an indication of reproducibility and magnitude of errors in measurement. The higher output current obtained with Combination V is due to the increased extraction voltage. On the basis of the 3/2 power law, an output current of 58 ma is to be expected as compared with Comb. IV and V. This is in fair agreement with the actual current obtained, i.e. 55 ma.

An examination of the emittance area plots (Figs. 10, 11 and 12) shows a pronounced boundary distortion for Combination V. With reference to an elliptical phase space boundary, distortions of the boundaries are connected with beam aberrations due to an imperfect optical system. For the case at hand, it is not likely that the more pronounced influence of aberrations is due to the extraction region. The higher extraction voltage results in a greater inward curvature of the plasma boundary with the result that the beam diameter in the extraction electrode aperture (3/16 inches here) certainly would not be larger than for Combinations III and IV. The voltage ratio for the following lens element was essentially the same for all three combinations. Therefore, the larger beam intensity with Combination V resulted in a larger filling of the F_2 electrode, entrance of column (see Fig. 1) region. As a consequence, the conclusion is that beam aberrations are mainly introduced in the F_2 electrode, entrance of column region and not in the extraction electrode region.

Combination VI. The large emittance area value obtained in this case is again considered to be due to the particular mode of operation of the duoplasmatron source, as indicated before. Geometrically and optically, this combination is almost identical with Combinations III, IV, and V, except for the larger wall thickness (T) of the plasma expansion cup. A comparison with following results indicates that this particular parameter is not responsible for the large emittance area value obtained here.

Combination VII. The results in this case form evidence that with optimum duoplasmatron conditions small emittance area values can be obtained with a 1/2 inch diameter extraction electrode aperture and

a 0.020 inches wall thickness of the plasma expansion cup. This is to be compared with Combinations I, II, and VI.

Comb. VIII, IX, X, XI. The dominant parameter in these cases was the depth of the plasma expansion cup. This has a pronounced influence on maximum obtainable output current. Also the emittance area value is significantly affected. Applying Langmuir's equation for a flat emitter

$$J_{\text{space charge limited}} = \frac{4\varepsilon_o}{9}\sqrt{\frac{2q}{m}}\,\frac{V^{3/2}}{d^2}$$

and using reasonable estimates for d, results in approximate values for optimum current density. Comparing this with current densities calculated from experimental results and with reference to the actual aperture diameter shows that in Combinations X and XI emission takes place from an area larger than the aperture hole area. The significant parameters and results are summarized in Table 4.

Table 4

Comb.	Aperture Hole area mm^2	L $(10^{-3}$ in.)	I_{tot} ma	d_{eff} cm	$V_{extr.}$ kv	$J_{sp.ch.l.}$ A/cm^2	$J_{exp.}\left(\frac{\text{re. hole}}{\text{area}}\right)$ A/cm^2	Area $F(y,\alpha_y)_{x=o}$ for 90% of I_{tot} mm-mrad
VIII	0.2	0	5	1.2	45	0.4	2.5	-
IX	1.2	0	38	0.4	40	2.8	3.2	-
X	0.2	55	30	0.6	43	1.2	15	135
XI	0.2	120	68	0.7	42	1.0	34	195
(XV	0.25	120	80	0.7	35	0.7	32	190)

The importance of the plasma expansion cup is obvious from these results. Higher extraction currents with the extraction fields used in the present preinjector are only obtained by allowing the plasma to expand, such that emission takes place over a larger area of the plasma boundary. Comparing results from Combinations VIII and XI, the increase in area might be as large as a factor of 10 as compared with actual source aperture area. If extraction takes place over a larger area of the plasma boundary, an increase in emittance area value is to be expected. Unfortunately, no emittance measurements were taken with Combination VIII, where this effect should have been most pronounced if compared with Combination XI. The same argument, to a lesser extent, holds for a comparison of Combination X and XI where the ratio in plasma boundary extraction area should be of the order of 2. Significantly, the ratio of resultant values of area $F(y,\alpha_y)_{x=o}$ for 90% I_{tot} is smaller than this factor and actually closer to 1.5.

The tabulated results indicate that in a first approximation the plasma density at the extraction boundary does not depend on the extent to which the plasma is allowed to expand, within limitations of the present experiment. Higher densities can be obtained simply with a change of duoplasmatron parameters. In that case with the extraction fields actually used, the boundary would attain such a shape, in order to satisfy the space charge limited extraction condition, that the resultant beam is unacceptable to extraction electrode (scraping of the beam) and following optical system.

Considering for the moment only the extraction region, it is obviously desirable, in order to keep the beam emittance area value small, to use the highest possible extraction fields. In this respect, it is interesting to compare the results of Combination V and XI where an

increase of current by 20% with higher extraction field (smaller gap distance) resulted actually in a slightly smaller emittance area value.

Combination XII. Using the same set of parameters as for Combination XI, except for a 30% larger aperture in the extraction electrode, results in a decrease in maximum output current of about 10%. If aberrations are mainly introduced in the extraction region a definite decrease in distortions of the phase space boundary would be expected. The opposite seems to be true (see Figures 16 and 17). This supports again the contention that aberrations are mainly introduced in the F_2 electrode, entrance of column region.

Combination XIII, XIV, XV. An attempt was made here to evaluate the influence of the extraction electrode length (S). This parameter determines, to a certain extent, the beam diameter in the F_2 electrode, entrance of column region. The results are abstracted from Table 1 and summarized below (Table 5).

Table 5

Comb.	Aperture Diam. (10^{-3} in.)	S (in.)	I_{tot} (ma)	$F(y,\alpha_y)_{x=o}$ for 90% of I_{tot} (mm-mrad)
XII	20	3.6	62	260
XIII	20	4.4	50	not measured
XIV	20	2.8	72	not measured
XV	25	2.8	80	190

Attempts to raise the output currents with the duoplasmatron parameters over the stated values resulted in breakdown in the focusing system due to fractional beam interception by the electrodes. It is significant, comparing Combinations XII and XV, that with the higher

output current obtained with Combination XV, a smaller emittance area was measured. Also the distortions due to aberrations seem to be reduced in this case (see Figures 17 and 18).

Combination XVI. Leaving all parameters the same except for source pressure, the output current was lowered by a factor of 2 as compared with Combination XV. It was unavoidable that the discharge current decreased by about 20%. The results indicate a lower emittance area value for lower output currents. This could be due to the fact that at lower source pressures, a less dense plasma could not exist in equilibrium with the same extraction fields, such that its shape changed and extraction would take place from a smaller area from a plasma of comparable density.

A priori, an equally valid argument would be the following. The influence of space charge forces being less at lower beam intensities would result in a smaller beam diameter in the F_2 electrode, entrance of column region, with consequent smaller aberrations of the beam. (Compare Figures 18 and 19.) This could result in a smaller phase space area assuming that the emittance area for Combination XV is enlarged due to aberrations, the silent assumption being made that Liouville's theorem is not applicable here because of coupled motion*. Lacking emittance area measurements for these combinations adjacent to the ion source rules out favoring either of these arguments.

As is clear from the results indicated in Table 2, in general, the density distribution in the phase space area is rather inhomogeneous. This is quantitatively expressed by taking the specific density for the emittance areas for 90% of I_{tot} and for 80% I_{tot}. These results together with the appropriate ratios (R) are given in Table 3. Obviously, for a

*This has been expanded in the afore-mentioned reference.

homogeneous density distribution, R should equal 1. The values of R do not show any apparent relationship with the total output current.

Loss of homogeneity in the phase space area observed at the 750 kev exit of the preinjector could be due to aberrations in the optical system. This could also be due to a non-homogeneous distribution of the plasma density within the area from which extraction takes place.

Considering spherical aberrations, this should be traced to two sources. First, true optical aberrations due to deficient external fields; second, spherical aberrations due to space charge forces in the beam. Considering first approximations, only in the case of a homogeneous beam would it be possible to consider the influence of space charge forces as a "negative lens", which could be compensated. In this case, homocentricity of the beam would be preserved. However, due to a potential difference in the beam between paraxial and peripheral ions, proportional to $(I/V^{1/2})$ a loss of homogeneity of the beam results. Especially in the extraction region, this effect could be pronounced at higher beam intensities. The loss of homogeneity of the beam, or the variation of current density with the transverse coordinate R leads to a beam expansion depending on the magnitude of R and thus the space charge equivalent lens depends on the angular aperture, hence spherical aberration.

As stated before, for all cases investigated, the density filling of the outer regions of the phase space area is relatively low. Therefore, with preinjector emittance area values larger than the linac acceptance area beam losses will not be in proportion to area ratios. Assuming optimum beam optical matching of preinjector to linac the value of beam current acceptable to the linac is calculated by assuming an elliptical acceptance area of 150 mm-mrad*. This was done by interpolation of the curves of emittance area versus percentage of I_{tot} as given in Fig. 20. These results are tabulated in Table 3 where both

*L. Smith, Internal Report, BNL, LS-3; D. Cohen, Internal Report, ANL, ANLAD-57

percentage of total current and absolute value of acceptable beam current is indicated. The assemption being made is that for the percentages given the corresponding phase space areas are nearly elliptical in shape. Especially for the higher output currents, this is a rough approximation only and the figures given should be considered as a first approximation only. Also, during operations, it was observed that, when using high preinjector currents, a fraction of this of up to 30% would be lost between pre-injector output and linac output. Nevertheless, the most favorable combination of parameters resulting in maximum acceptable beam current is obvious again from the tabulated results.

Since performing the measurements described above, some results of emittance area measurements with the duoplasmatron source became available from Argonne National Laboratory* and from Lawrence Radiation Laboratory**.

At ANL, emittance area measurements only were done with visual observation of the shadow image of a series of slits placed in the beam, at a beam energy of 200 kev. The resultant values are converted to 750 kev for comparison with the present results. This is indicated by upside-down triangles (▽) in Figs. 21a and 21b. Because of the method used, it is difficult to assess what fraction of the total beam would be represented by the areas indicated. Resultant emittance area values are comparable in magnitude as those obtained here. Extraction voltages were of the order of 30 to 40 kv for similar extraction gap distances.

The results obtained at LRL indicate emittance area values for relative high current outputs, obtained at 375 kev beam energy. These are again converted to 750 kev for comparison with the present results. This is indicated by normal triangles in Fig. 21a. The emittance area values were obtained with the four-slit method and represent approximately

---

* A. Yokosawa, R. McKeever, Internal Report, ANL, AY-RM 1

** R.W. Allison et al., LRL, Report UCRL-9743

95% of I_{tot}. The results are comparable to those or follow the same trend as those obtained here with the most favorable combination of parameters. Somewhat higher extraction fields were used (70 kv for similar geometry as used here).

The optical system following the ion source used here and that used at LRL is quite different, nevertheless, the combined results follow the same trend of increasing emittance area value with output current. This suggests strongly that the emittance area values are established before entering the optical system and that aberrations may distort the emittance area boundaries but do not affect the areas to a pronounced extent.

Summary of Results and Future Work

The preinjector output current was investigated with the duoplasmatron source as ion source. Phase space area, phase space density distribution and maximum obtainable output currents were observed for various combinations of extraction region geometrical and duoplasmatron parameters. In general, increasing the beam intensity by a factor of two results in an increase of the corresponding phase space area by about the same factor except for the most favorable combination of parameters where this factor might approach 1.5.

With limited extraction fields, it is necessary, in order to obtain high output currents from the duoplasmatron source, to use a plasma expansion cup.

With similar extraction fields, beam extraction takes place from plasmas of nearly equal densities. Higher output currents can be obtained at the cost of an enlargement in boundary area over which extraction takes place. This is in order to satisfy the space charge limited extraction condition.

Substantially higher plasma densities than actually used can be obtained with the duoplasmatron source but do result in beam optical conditions which are unacceptable to the present preinjector focusing system.

The present results indicate that higher extraction fields do promote larger output currents without enlarging the corresponding phase space area. In order to obtain a focused beam, present extraction voltages are limited by the maximum voltage maintainable at the F_1 electrode.

Aberrations introduced in the F_2 electrode, entrance of column region are mostly responsible for distortions of the observed phase space area boundary. Possibly for the same reason nonhomogeneous density distributions are observed in the phase space area representation.

Having evaluated a favorable combination of parameters for duoplasmatron and extraction region geometry, a short term approach will be to concentrate on improving the optical system such that higher extraction voltages could be employed. Also, aberrations in the F_2 electrode, entrance of column region should be reduced to a minimum, either by shaping the external fields or reducing the beam diameter in this region. In the latter case, it is unavoidable that the optimum optical entrance conditions (r and dr/dz) of the accelerator column, for a certain current input, cannot be matched. It is possible, however, to correct for this with the electrostatic lens at the 750 kev end of the column. Also, the entrance conditions could be changed with some high gradient sections at the entrance of the column. A further possibility exists to increase the over-all voltage gradient by means of shortening the accelerator column.

In connection with aberrations in the F_2 electrode, entrance of column region, it is interesting to note that previous computer calculations tracing the beam periphery through the total preinjector, indicated that at currents of approximately 100 ma, the beam diameter at the entrance of the column, when properly matched, would have approximately the same value as the actual geometrical aperture in this region.

A longer term approach to the problem of high preinjector beam intensity with low emittance area value calls for a computational study of relative merits of various over-all focusing systems, using as an entrance condition a beam of certain intensity with corresponding experimentally measured phase space area and phase space density distribution, obtained with highest possible extraction fields from the duoplasmatron ion source.

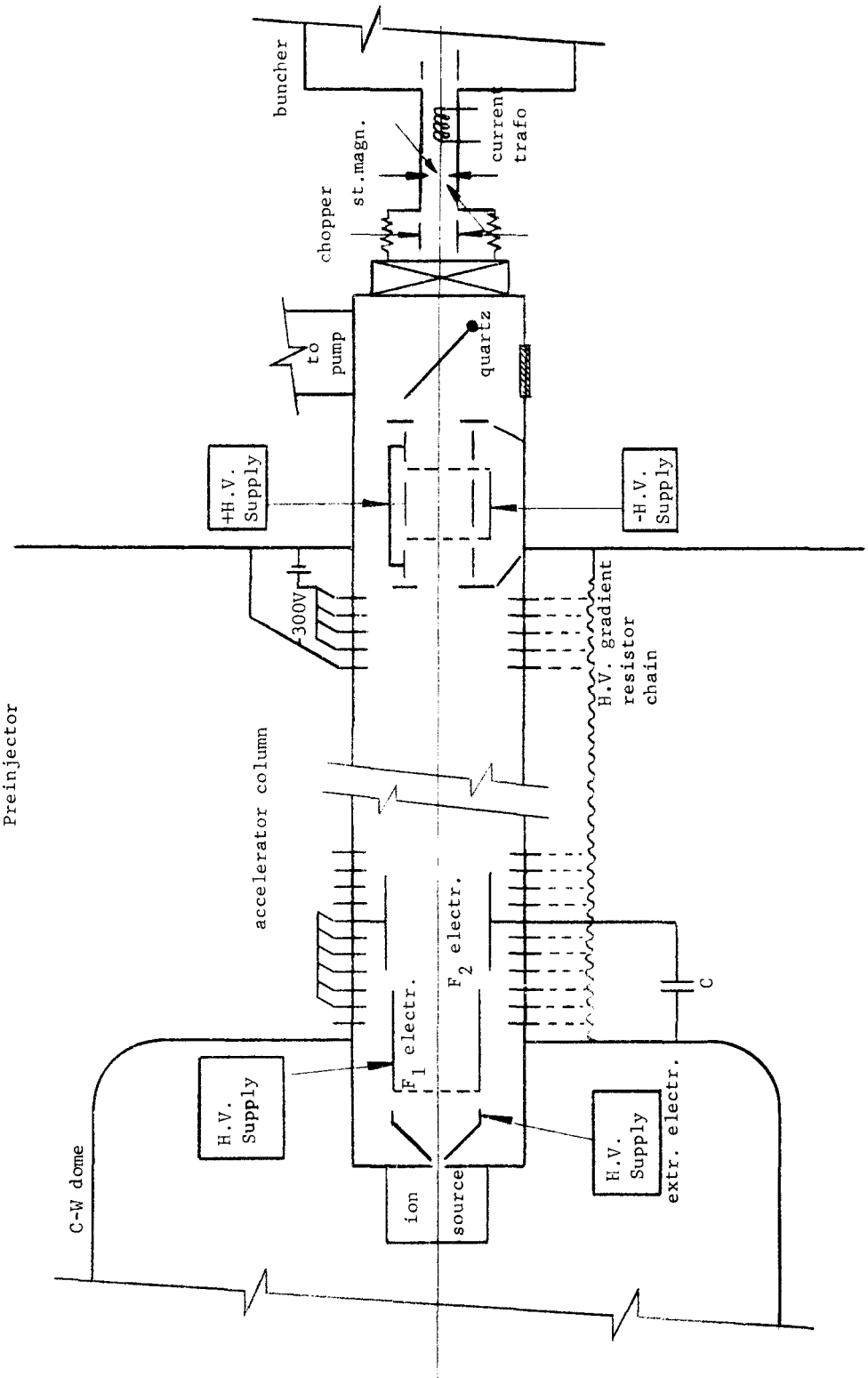

Fig. 1 Preinjector

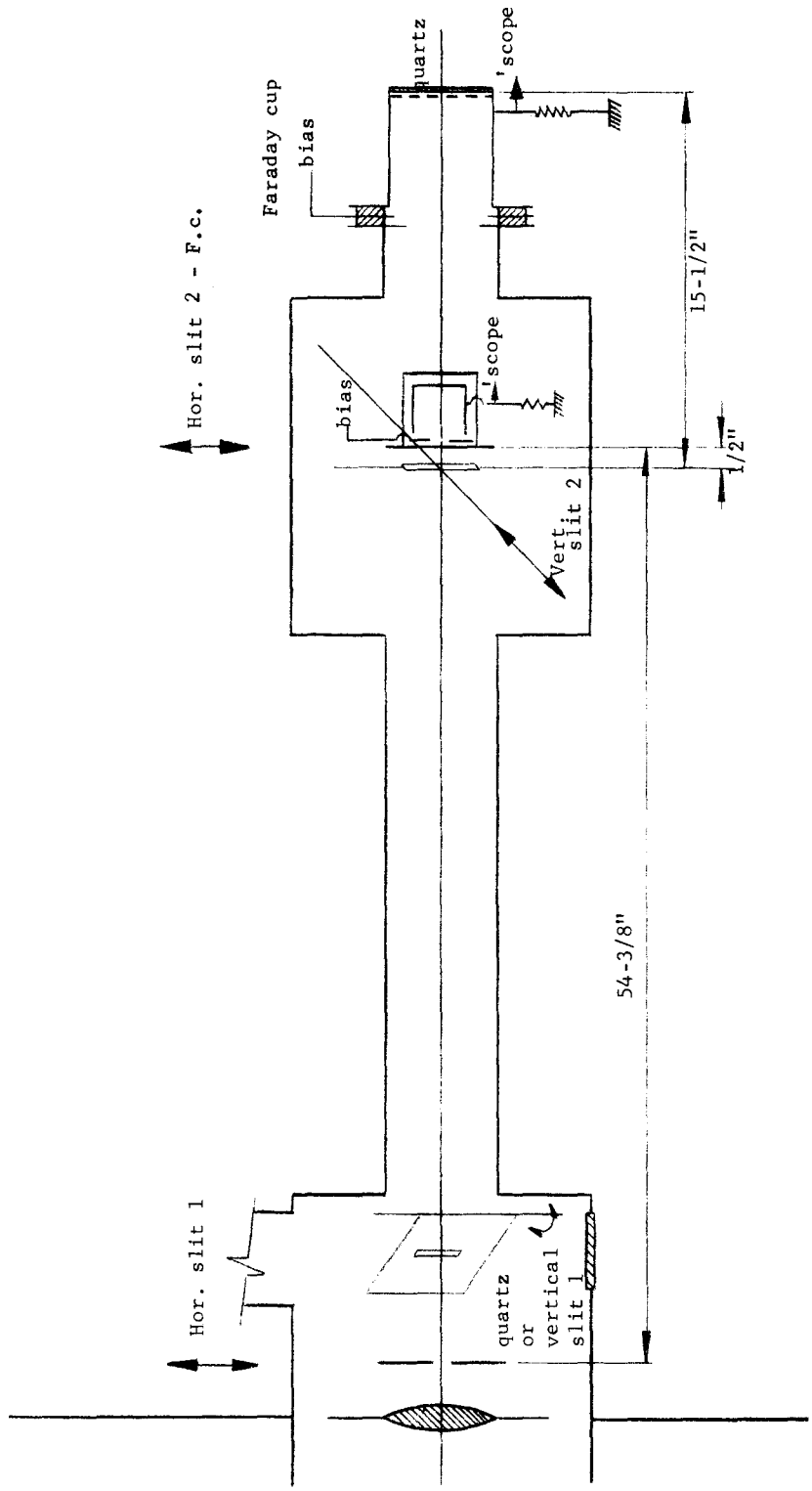

Fig. 2

Experimental arrangement

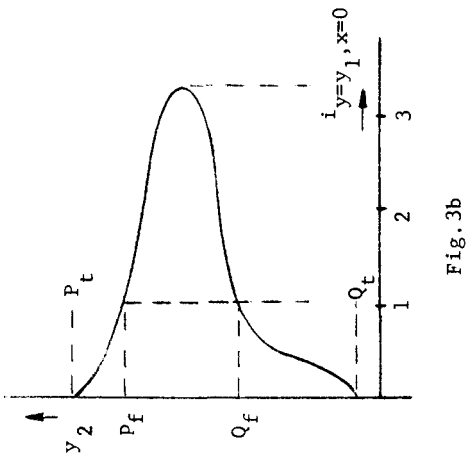

Fig. 3b

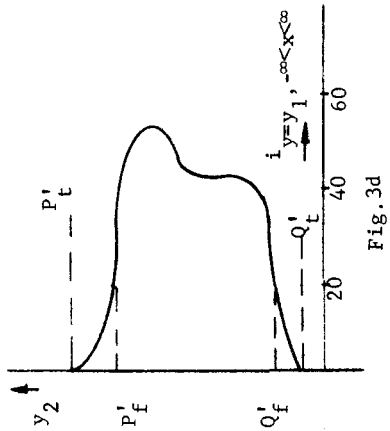

Fig. 3d

Fig. 3

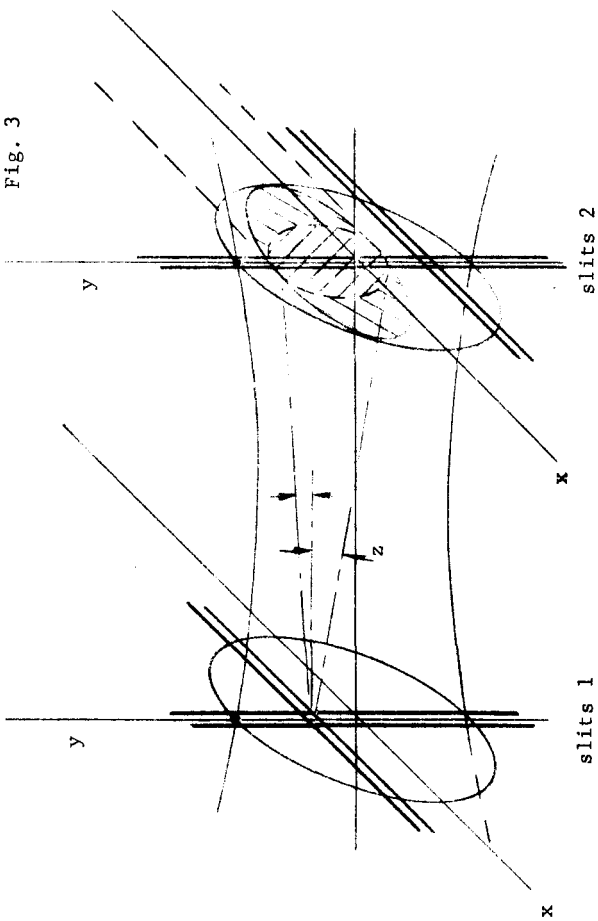

Fig. 3a

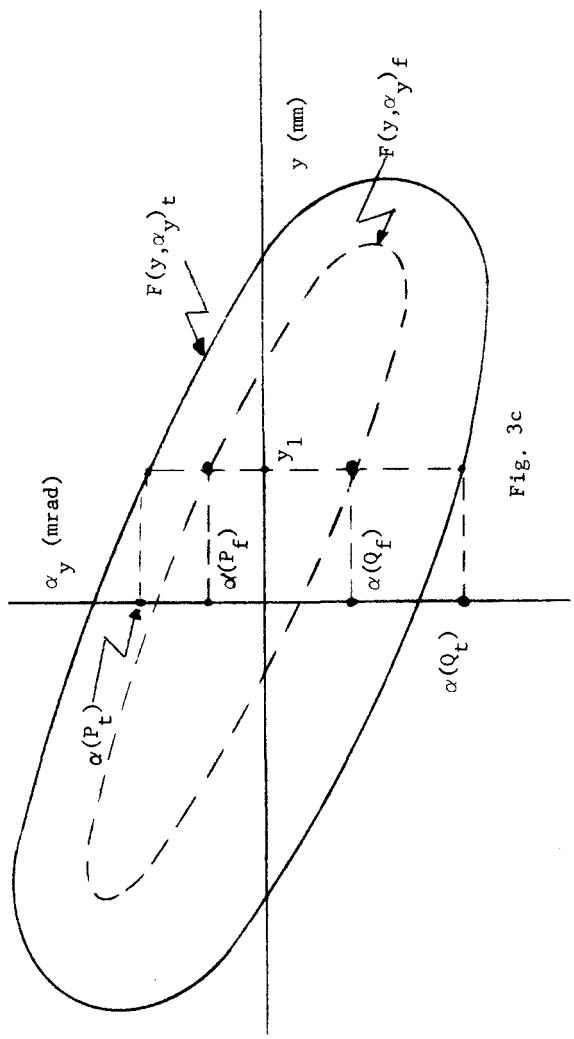

Fig. 3c

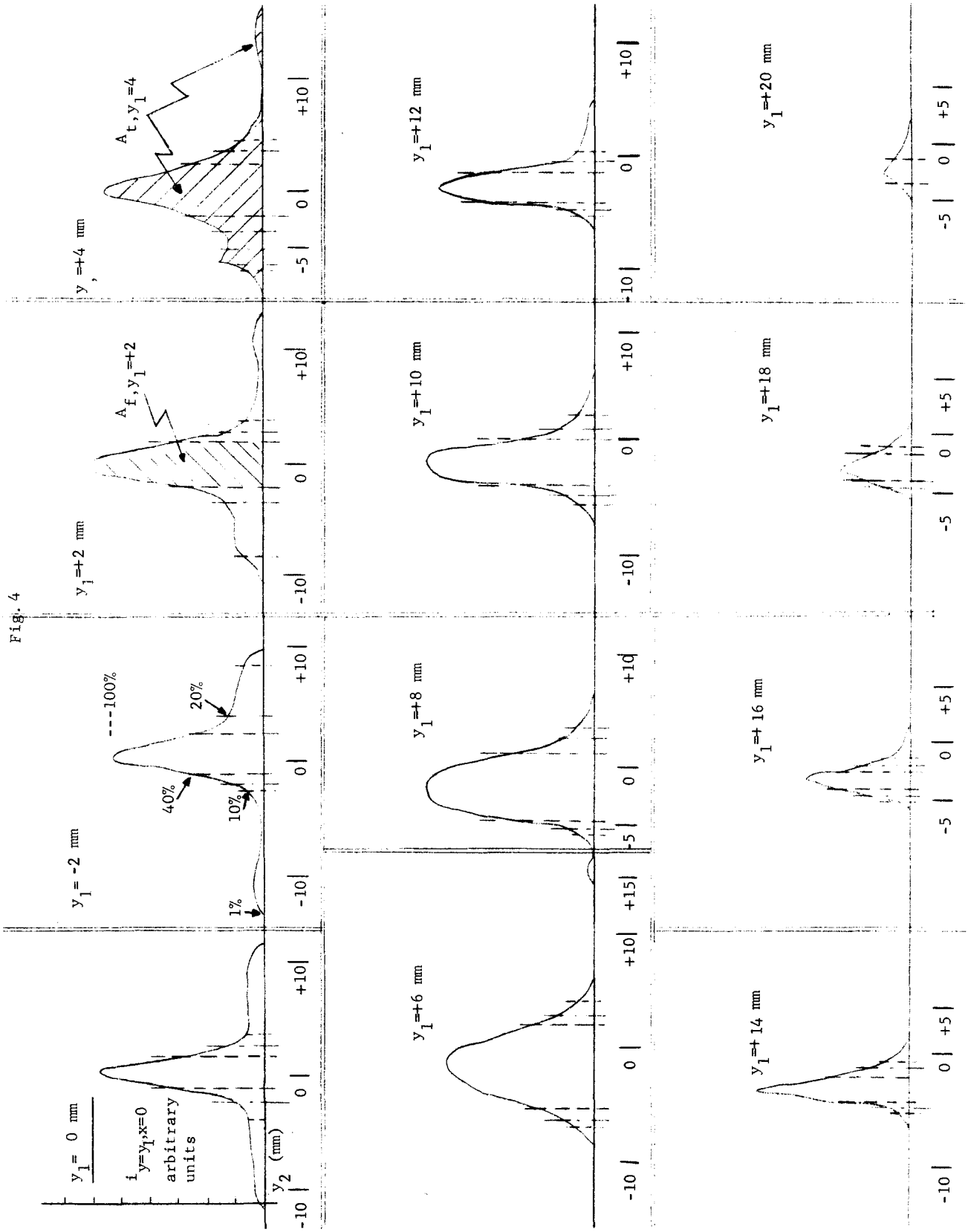
y1= 0 mm
i y=y1,x=0 arbitrary units
y2 (mm)
y1= -2 mm
---100%
20%
40%
10%
1%
y1=+2 mm
At,y1=+4
Af,y1=+2
y1=+4 mm
y1=+6 mm
y1=+8 mm
y1=+10 mm
y1=+12 mm
y1=+14 mm
y1=+16 mm
y1=+18 mm
y1=+20 mm

Fig. 4

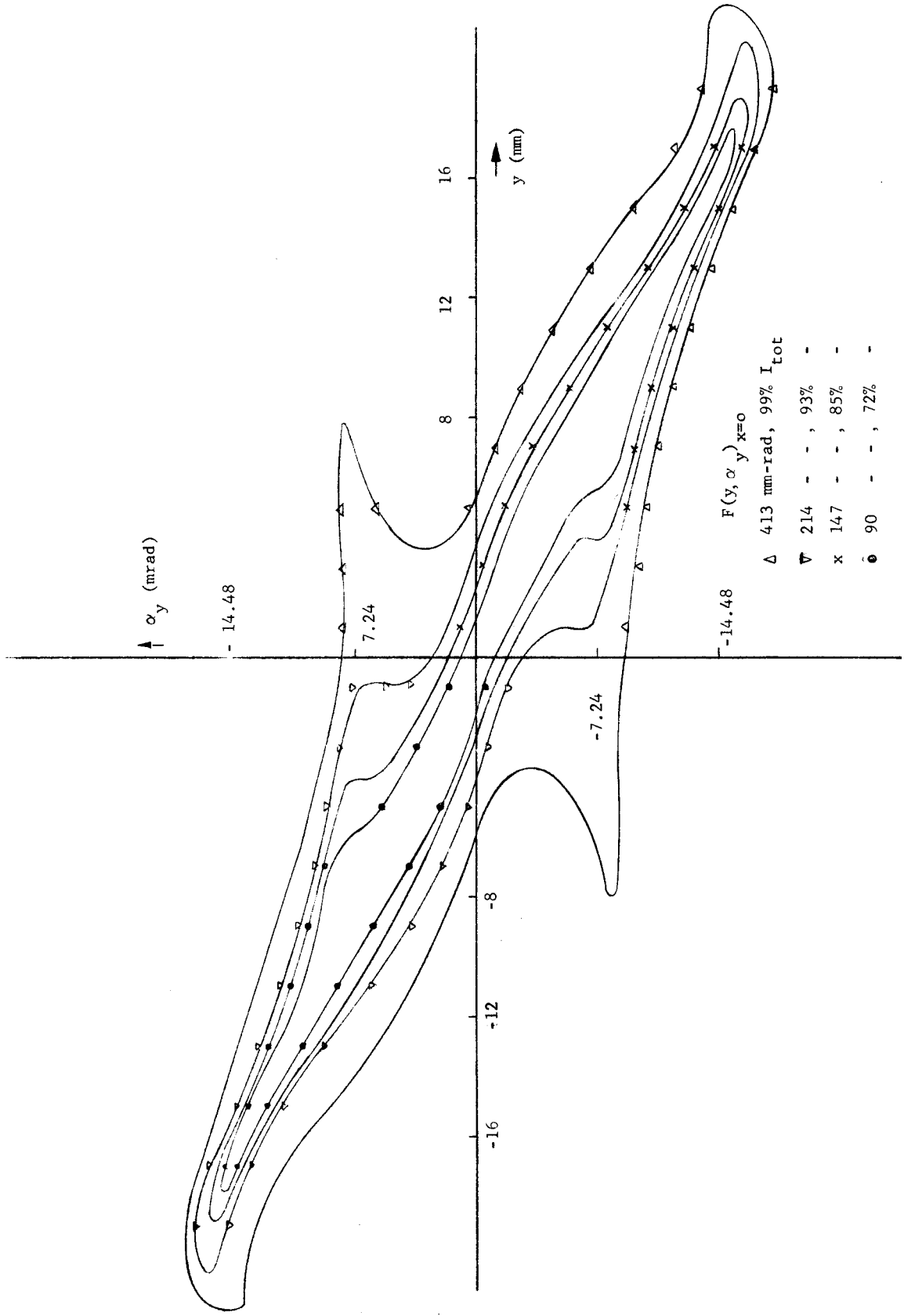
16
12
8
y (mm)
-8
-12
-16
α_y (mrad)
- 14.48
7.24
-7.24
-14.48
$F(y, \alpha_y)_{x=o}$
Δ 413 mm-rad, 99% I_{tot}
▽ 214 - - , 93% -
x 147 - - , 85% -
● 90 - - , 72% -

Fig. 5

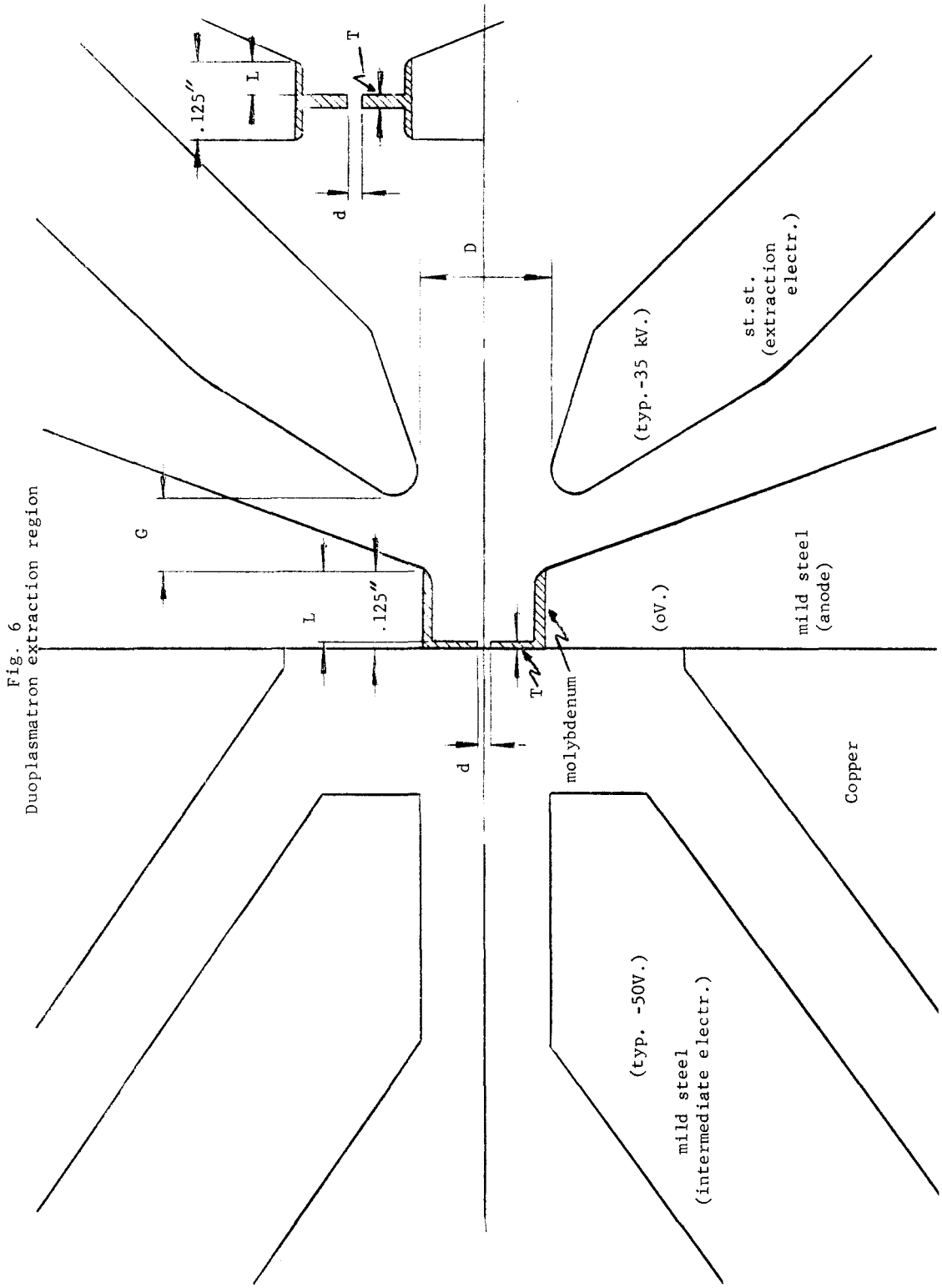

Fig. 6
Duoplasmatron extraction region

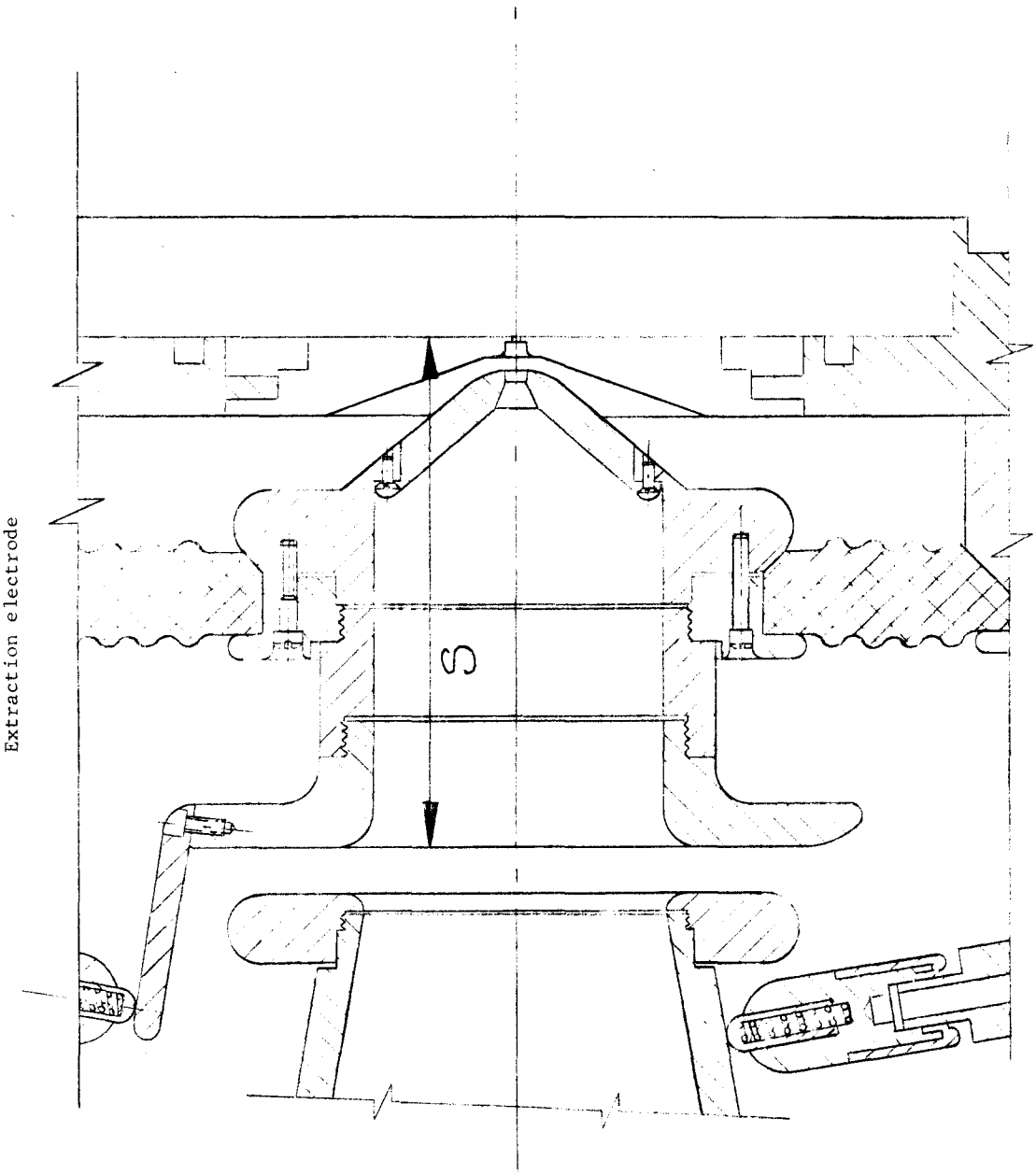

Fig. 7
Extraction electrode

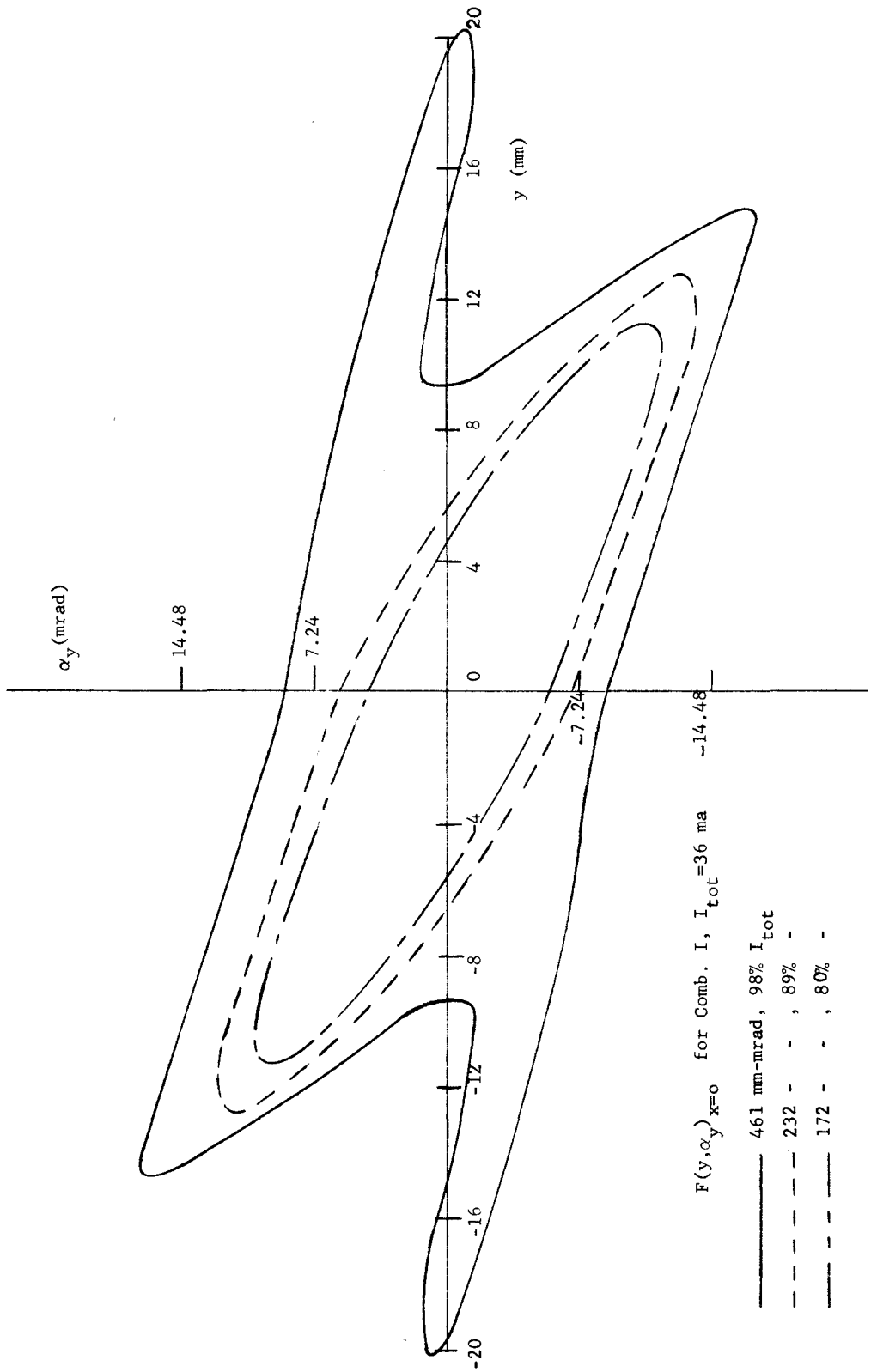
20
16
12
8
4
0
-4
-8
-12
-16
-20
y (mm)
α_y (mrad)
14.48
7.24
-7.24
-14.48
$F(y,\alpha_y)_{x=o}$ for Comb. I, I_{tot}=36 ma
461 mm-mrad, 98% I_{tot}
232 - - , 89% -
172 - - , 80% -

Fig. 8

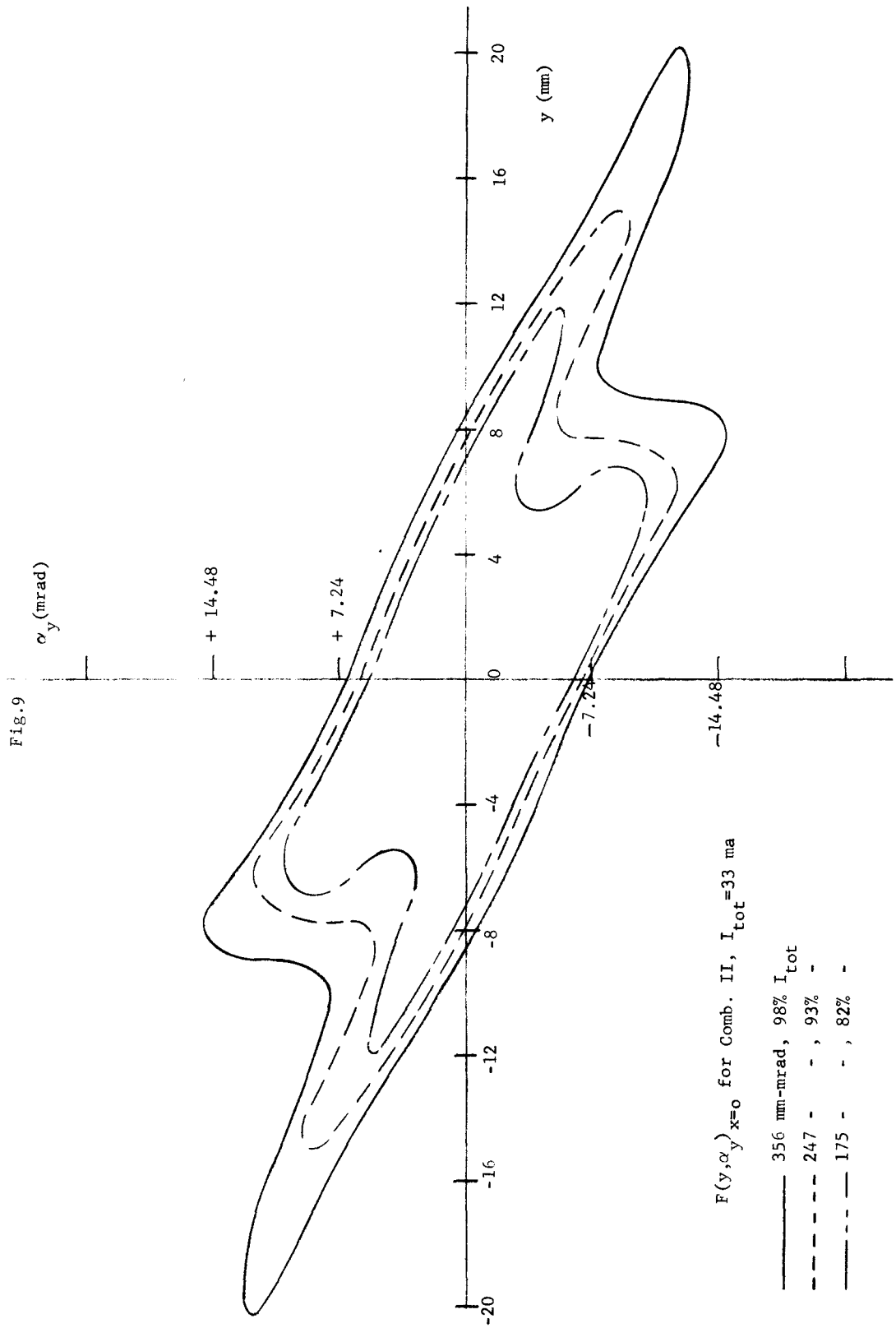
y (mm)
20
16
12
8
4
0
-4
-8
-12
-16
-20
α_y (mrad)
+ 14.48
+ 7.24
−7.24
−14.48
$F(y,\alpha_y)_{x=o}$ for Comb. II, I_{tot}=33 ma
356 mm-mrad, 98% I_{tot}
247 - - , 93% -
175 - - , 82% -

Fig.9

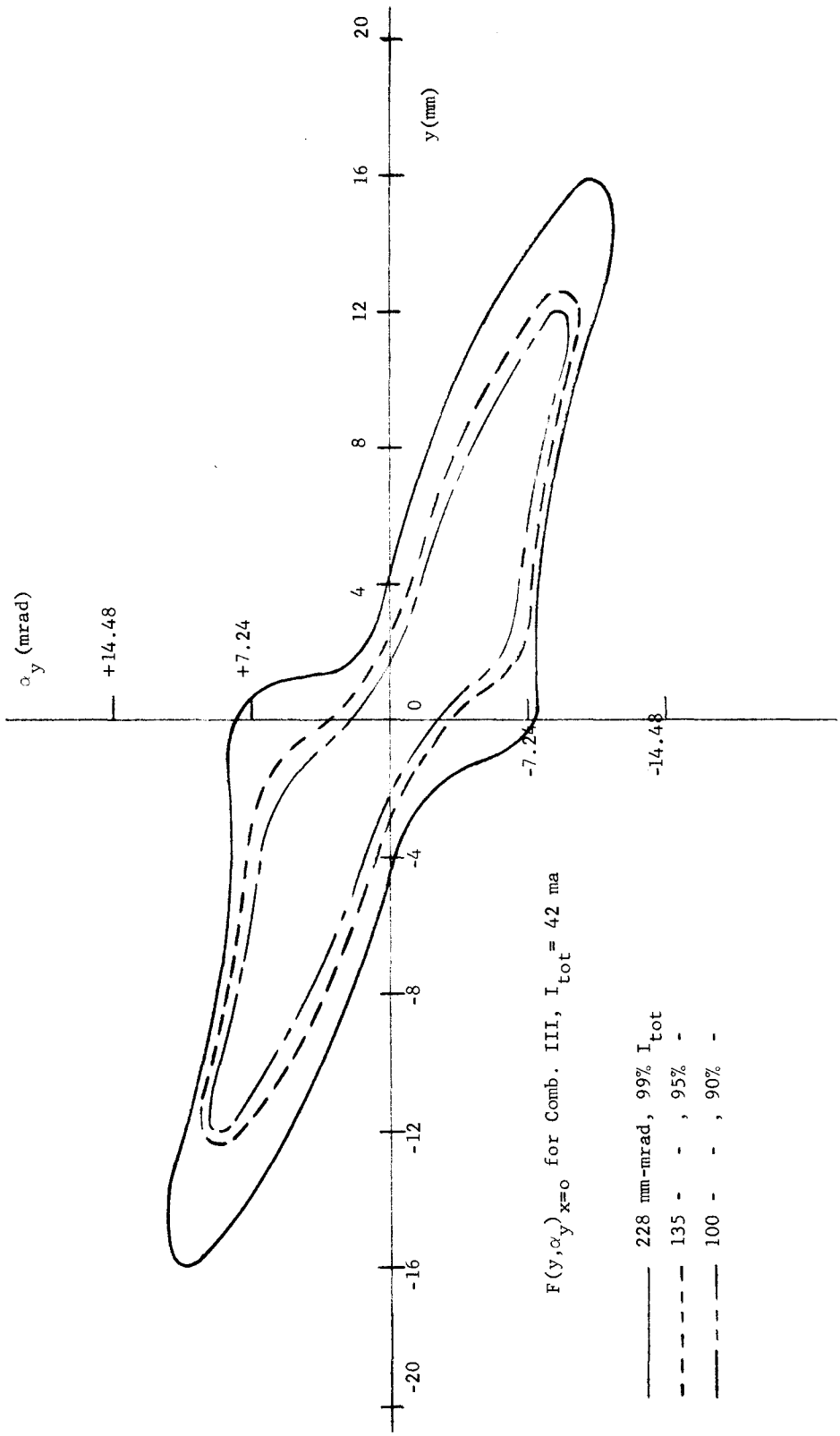
y (mm)
20
16
12
8
4
0
-4
-8
-12
-16
-20
α_y (mrad)
+14.48
+7.24
-7.24
-14.48
$F(y,\alpha_y)_{x=o}$ for Comb. III, I_{tot} = 42 ma
228 mm-mrad, 99% I_{tot}
135 - - , 95% -
100 - - , 90% -

Fig. 10

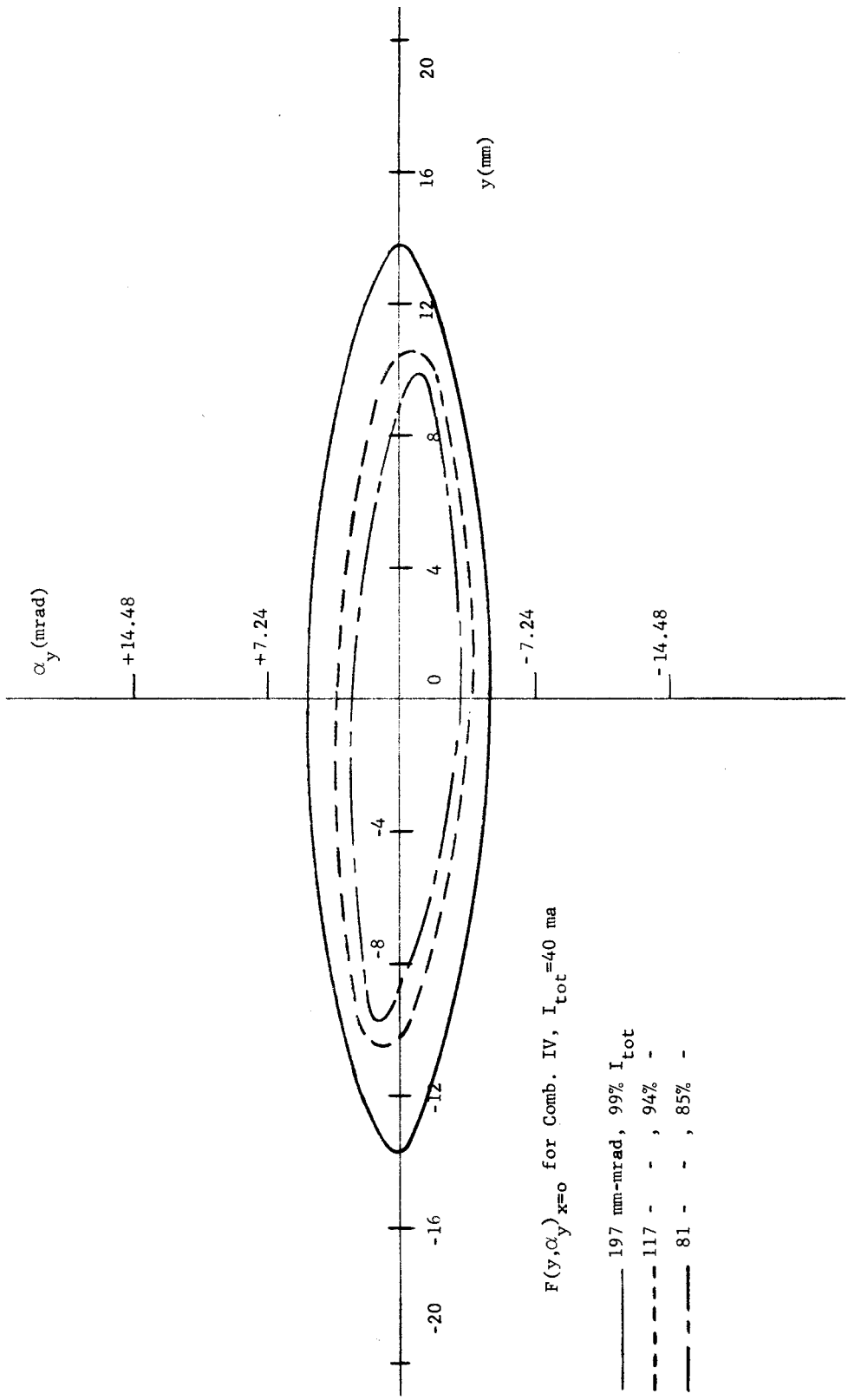
α_y (mrad)
+14.48
+7.24
-7.24
-14.48
y (mm)
20
16
12
8
4
0
-4
-8
-12
-16
-20
$F(y,\alpha_y)_{x=o}$ for Comb. IV, I_{tot}=40 ma
197 mm-mrad, 99% I_{tot}
117 - - , 94% -
81 - - , 85% -

Fig.11

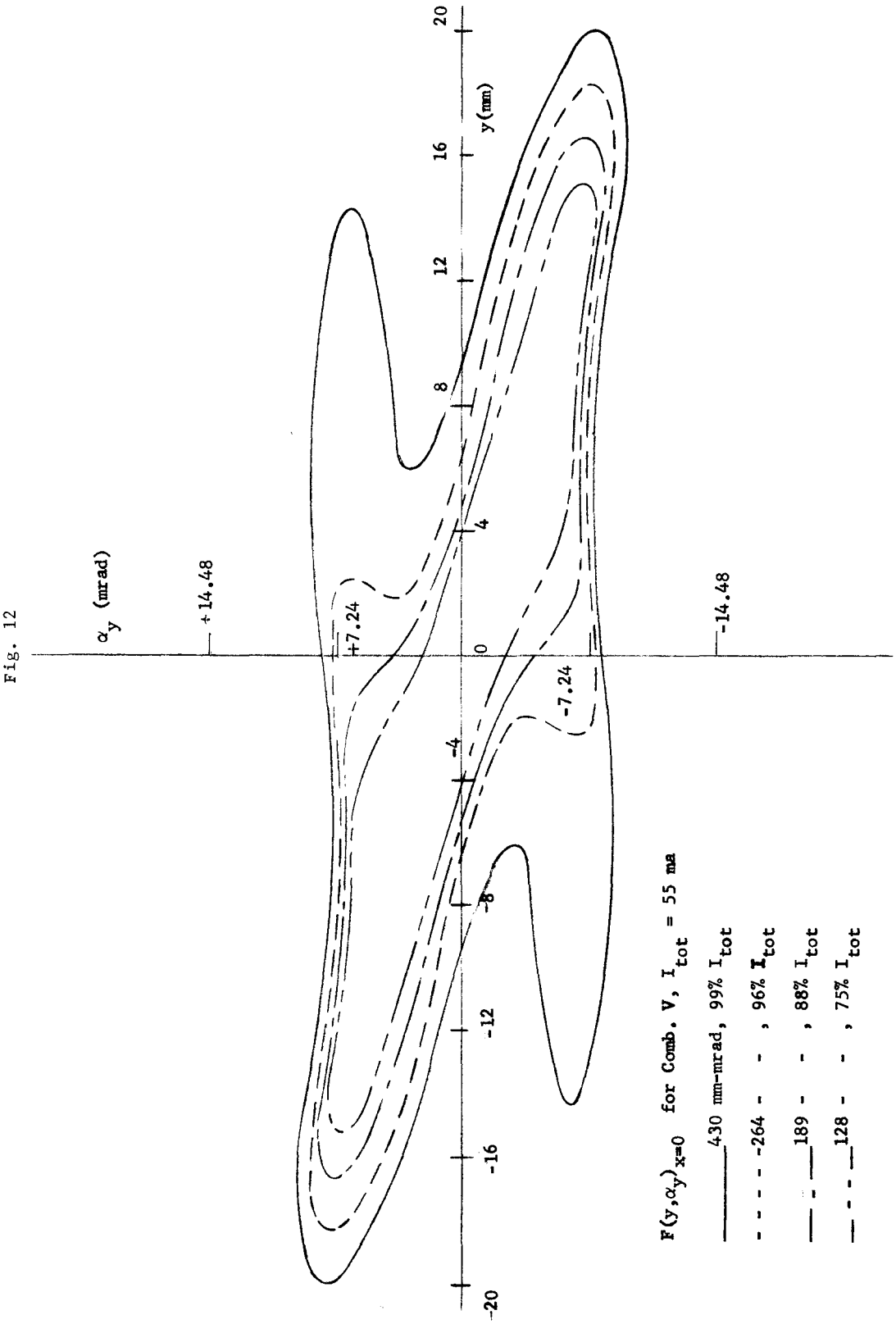
Fig. 12
α_y (mrad)
+14.48
+7.24
-7.24
-14.48
y(mm)
20
16
12
8
4
0
-4
-8
-12
-16
-20
$F(y,\alpha_y)_{x=0}$ for Comb. V, I_{tot} = 55 ma
430 mm-mrad, 99% I_{tot}
-264 - - , 96% I_{tot}
189 - - , 88% I_{tot}
128 - - , 75% I_{tot}

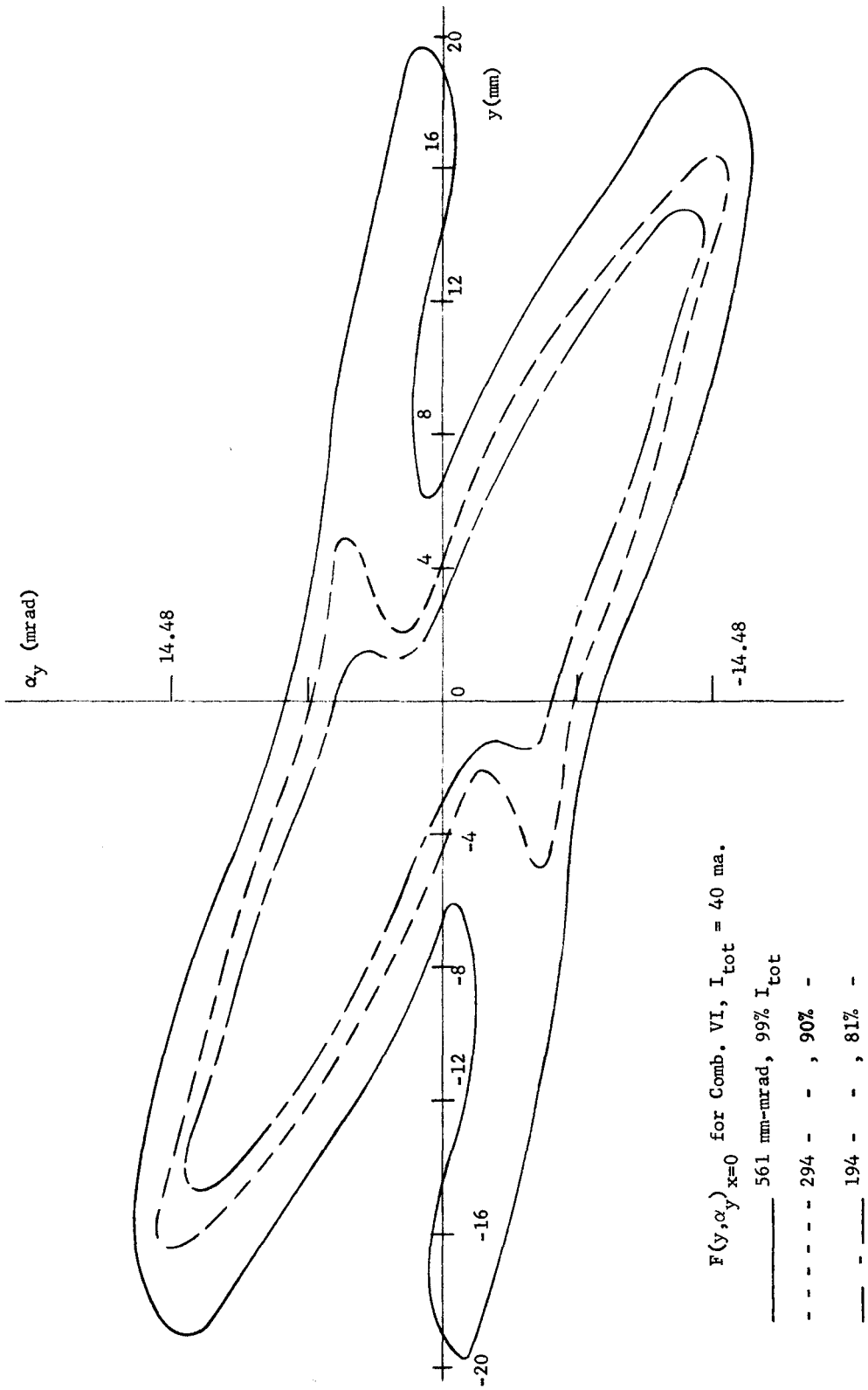
α_y (mrad)
14.48
-14.48
0
y (mm)
20
16
12
8
4
-4
-8
-12
-16
-20
$F(y,\alpha_y)_{x=0}$ for Comb. VI, I_{tot} = 40 ma.
561 mm-mrad, 99% I_{tot}
294 - - , 90% -
194 - - , 81% -

Fig. 13

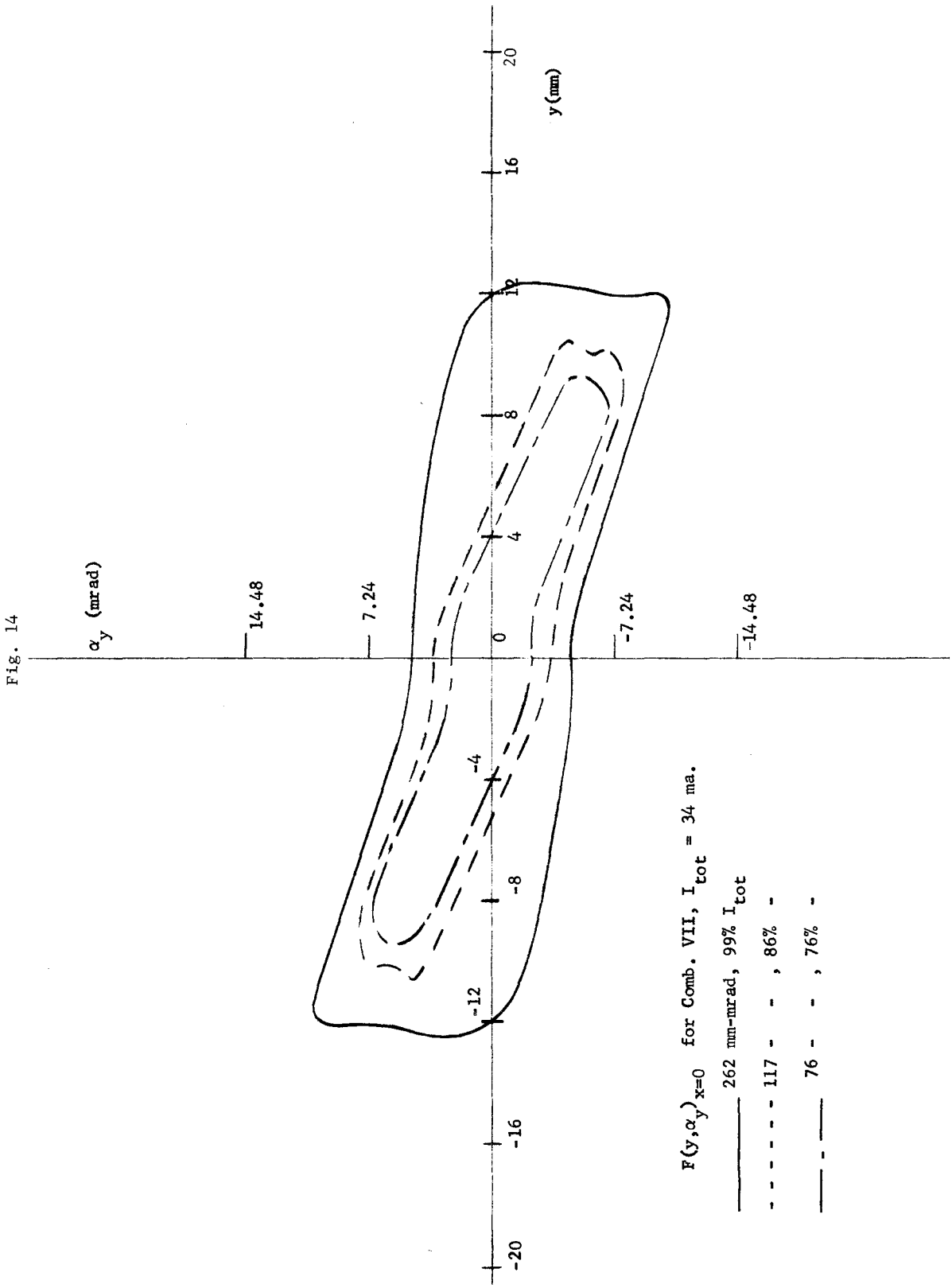
y (mm)
20
16
12
8
4
0
-4
-8
-12
-16
-20
α_y (mrad)
14.48
7.24
-7.24
-14.48
$F(y,\alpha_y)_{x=0}$ for Comb. VII, I_{tot} = 34 ma.
262 mm-mrad, 99% I_{tot}
117 - - , 86% -
76 - - , 76% -

Fig. 14

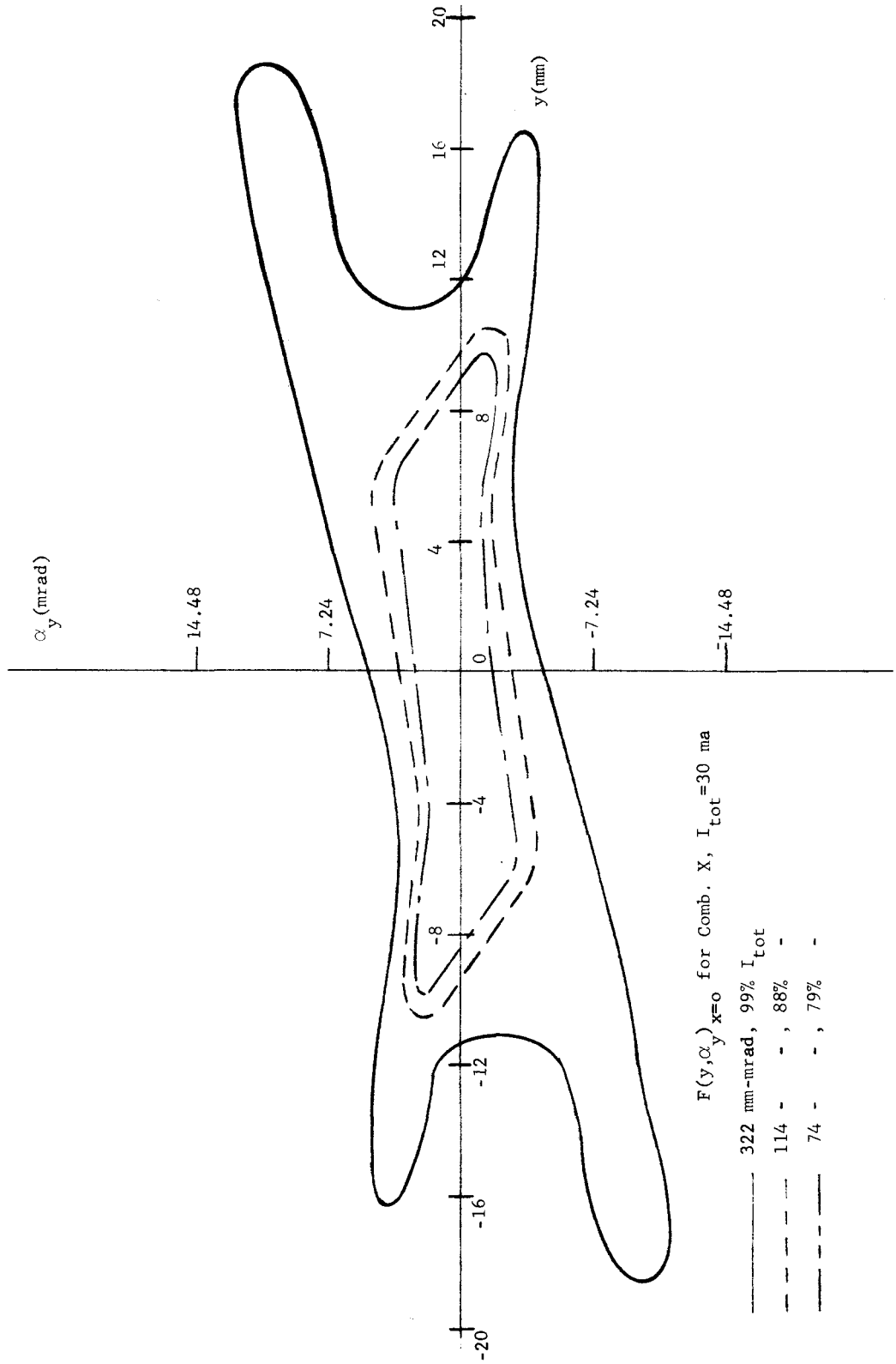
y (mm)
20
16
12
8
4
0
-4
-8
-12
-16
-20
α_y (mrad)
14.48
7.24
-7.24
-14.48
$F(y,\alpha_y)_{x=o}$ for Comb. X, I_{tot}=30 ma
322 mm-mrad, 99% I_{tot}
114 - - , 88% -
74 - - , 79% -

Fig. 15

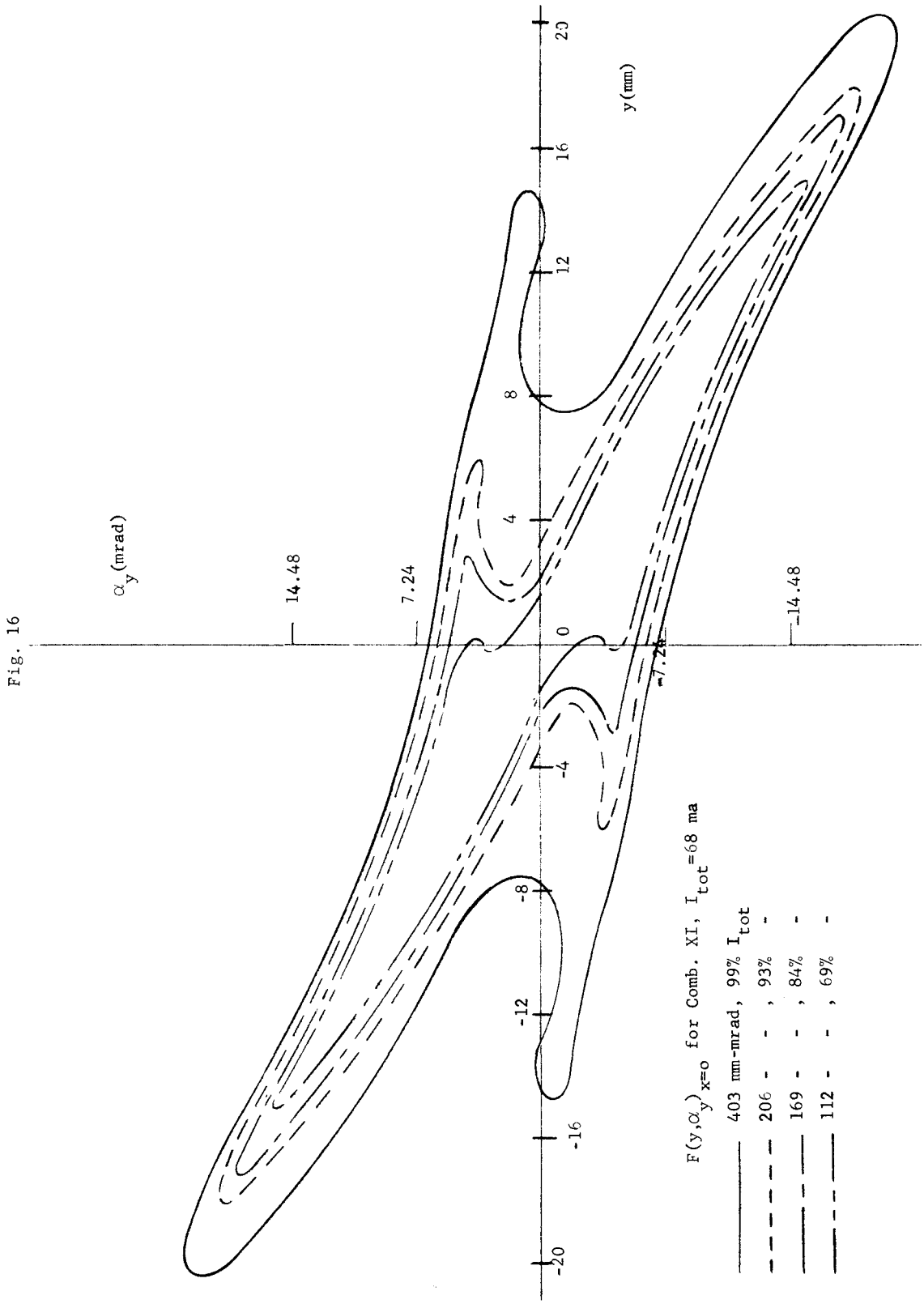
y (mm)
20
16
12
8
4
0
-4
-8
-12
-16
-20
α_y (mrad)
14.48
7.24
-7.24
-14.48
$F(y,\alpha_y)_{x=o}$ for Comb. XI, I_{tot}=68 ma
403 mm-mrad, 99% I_{tot}
206 - - , 93% -
169 - - , 84% -
112 - - , 69% -

Fig. 16

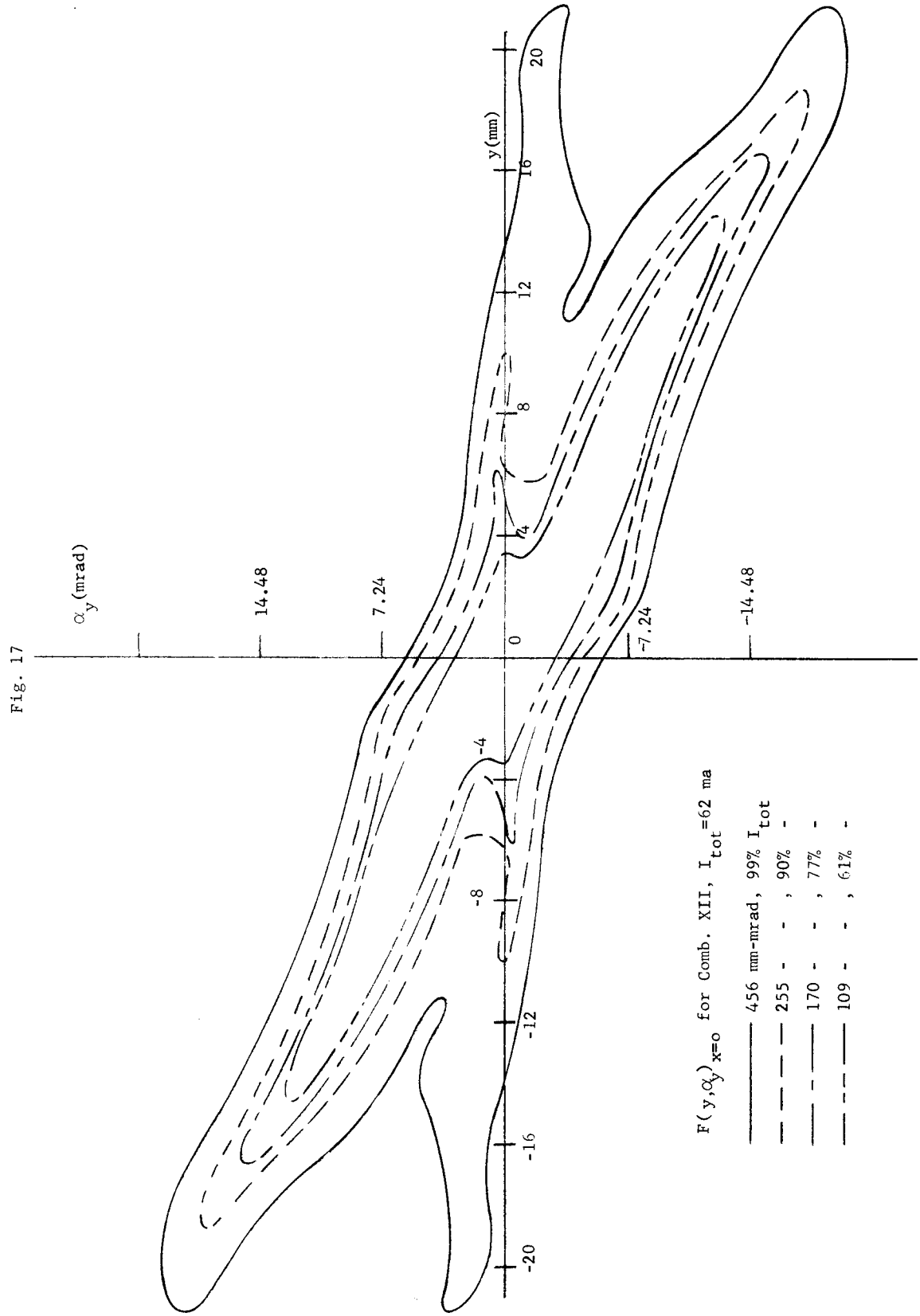
α_y (mrad)
14.48
7.24
0
-7.24
-14.48
y (mm)
20
16
12
8
4
-4
-8
-12
-16
-20
$F(y,\alpha_y)_{x=0}$ for Comb. XII, I_{tot}=62 ma
456 mm-mrad, 99% I_{tot}
255 - - , 90% -
170 - - , 77% -
109 - - , 61% -

Fig. 17

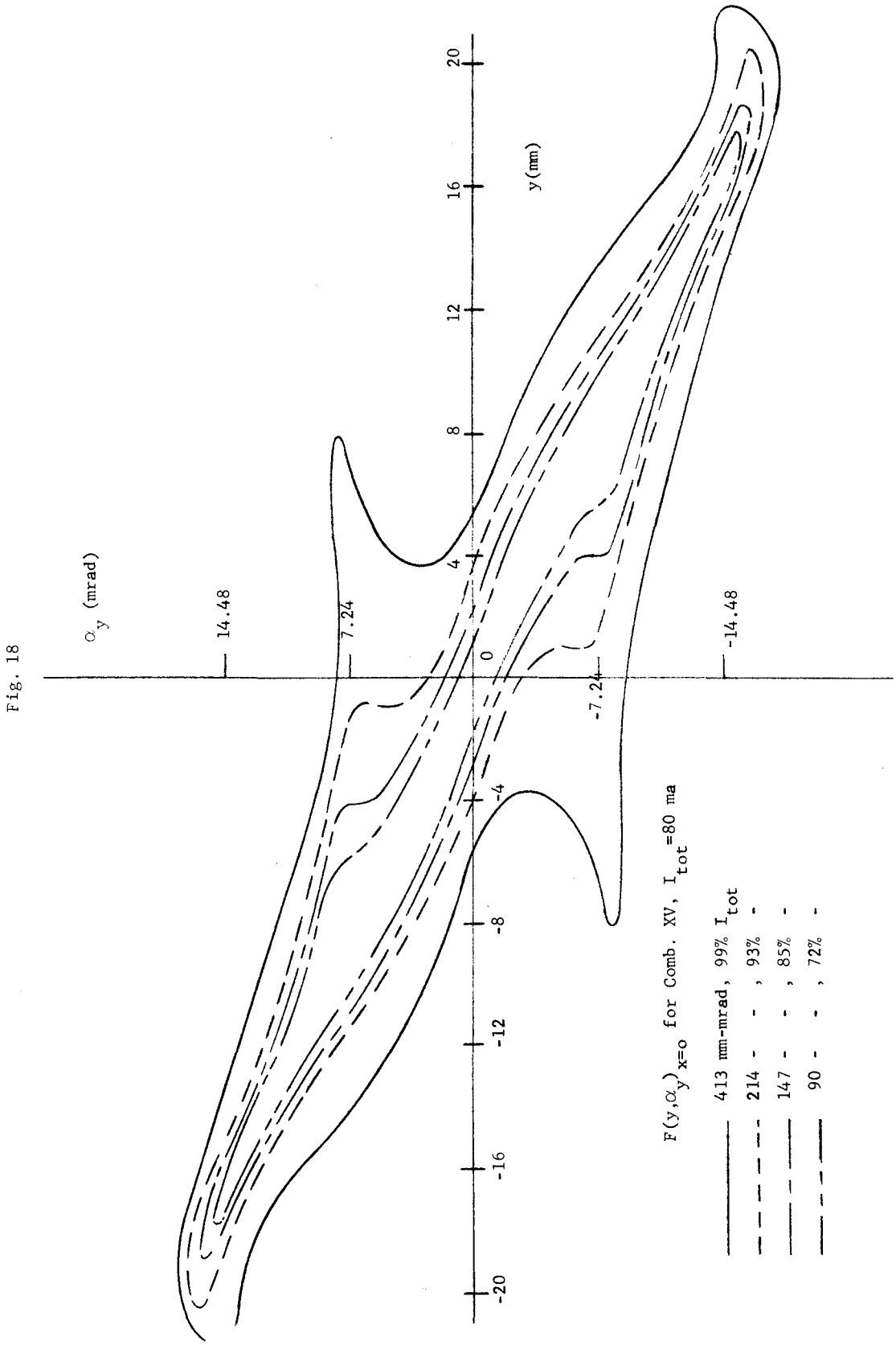
α_y (mrad)
14.48
7.24
-7.24
-14.48
y (mm)
20
16
12
8
4
0
-4
-8
-12
-16
-20
$F(y,\alpha_y)_{x=o}$ for Comb. XV, I_{tot}=80 ma
413 mm-mrad, 99% I_{tot}
214 - - , 93% -
147 - - , 85% -
90 - - , 72% -

Fig. 18

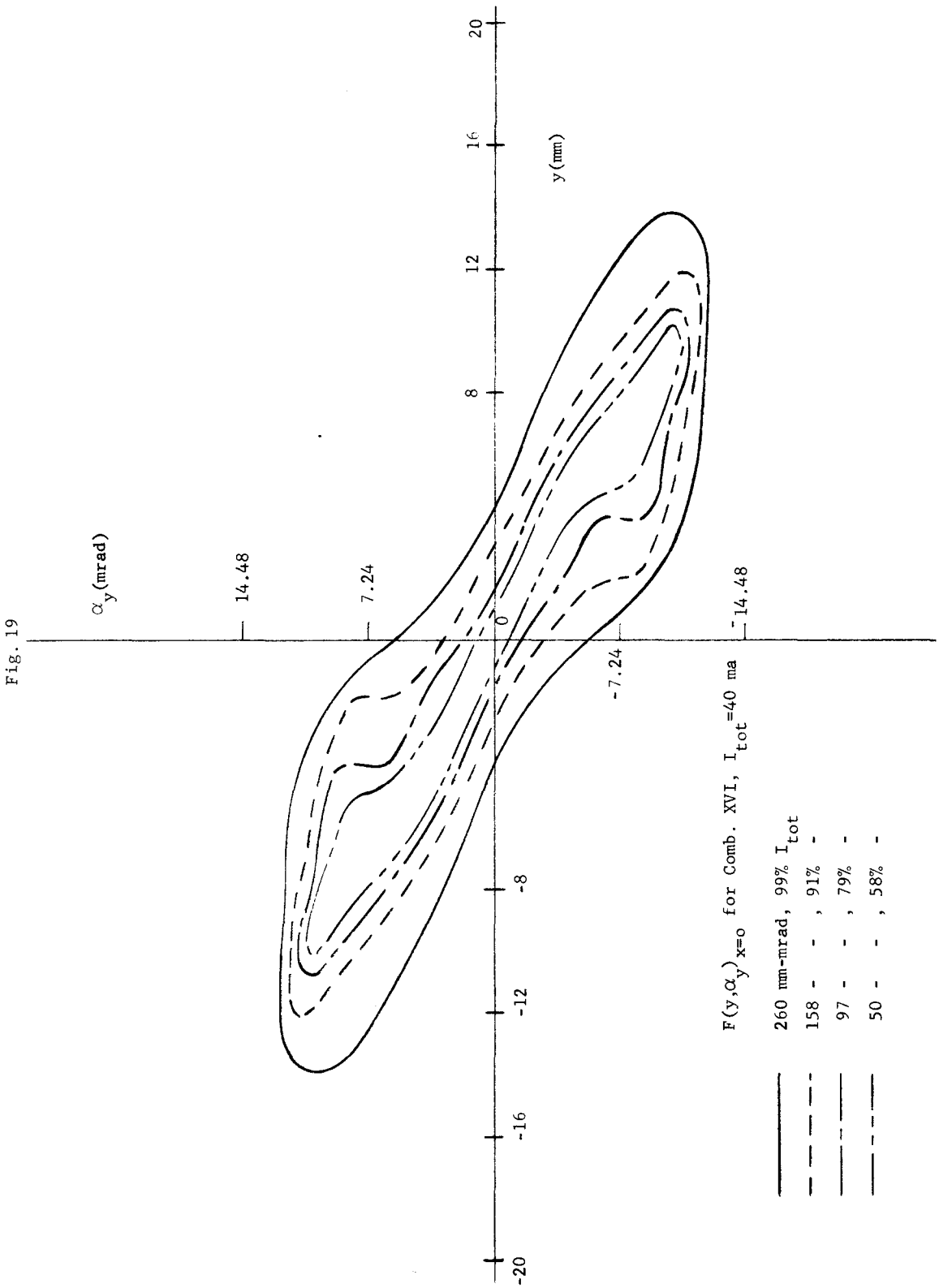
20
16
12
8
y(mm)
α_y(mrad)
14.48
7.24
0
-7.24
-14.48
-8
-12
-16
-20
$F(y,\alpha_y)_{x=o}$ for Comb. XVI, I_{tot}=40 ma
260 mm-mrad, 99% I_{tot}
158 - - , 91% -
97 - - , 79% -
50 - - , 58% -

Fig. 19

Fig. 20

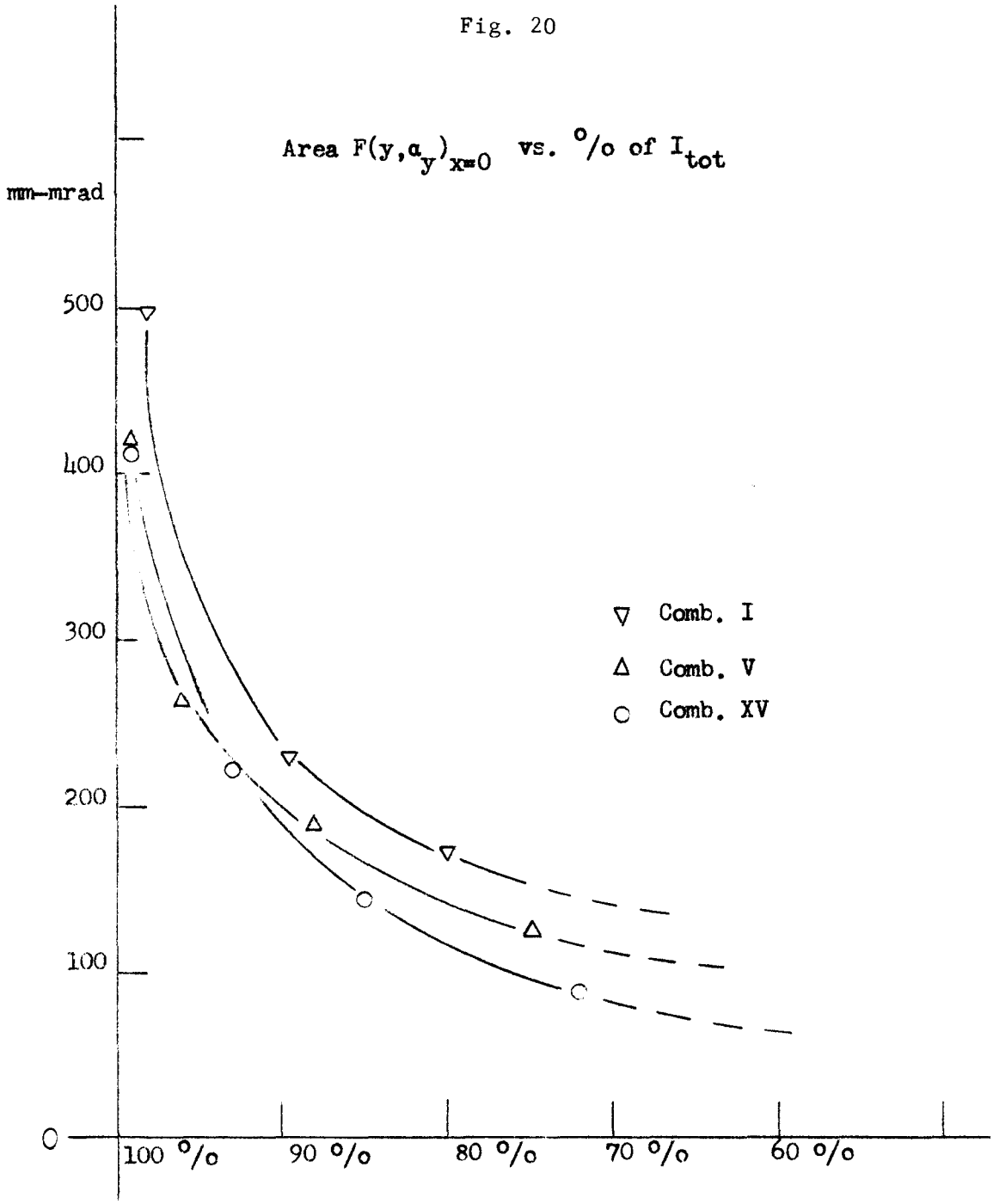
Area $F(y,\alpha_y)_{x=0}$ vs. °/o of I_{tot}
mm-mrad
500
400
300
200
100
0
100 °/o
90 °/o
80 °/o
70 °/o
60 °/o
Comb. I
Comb. V
Comb. XV

Fig. 21a

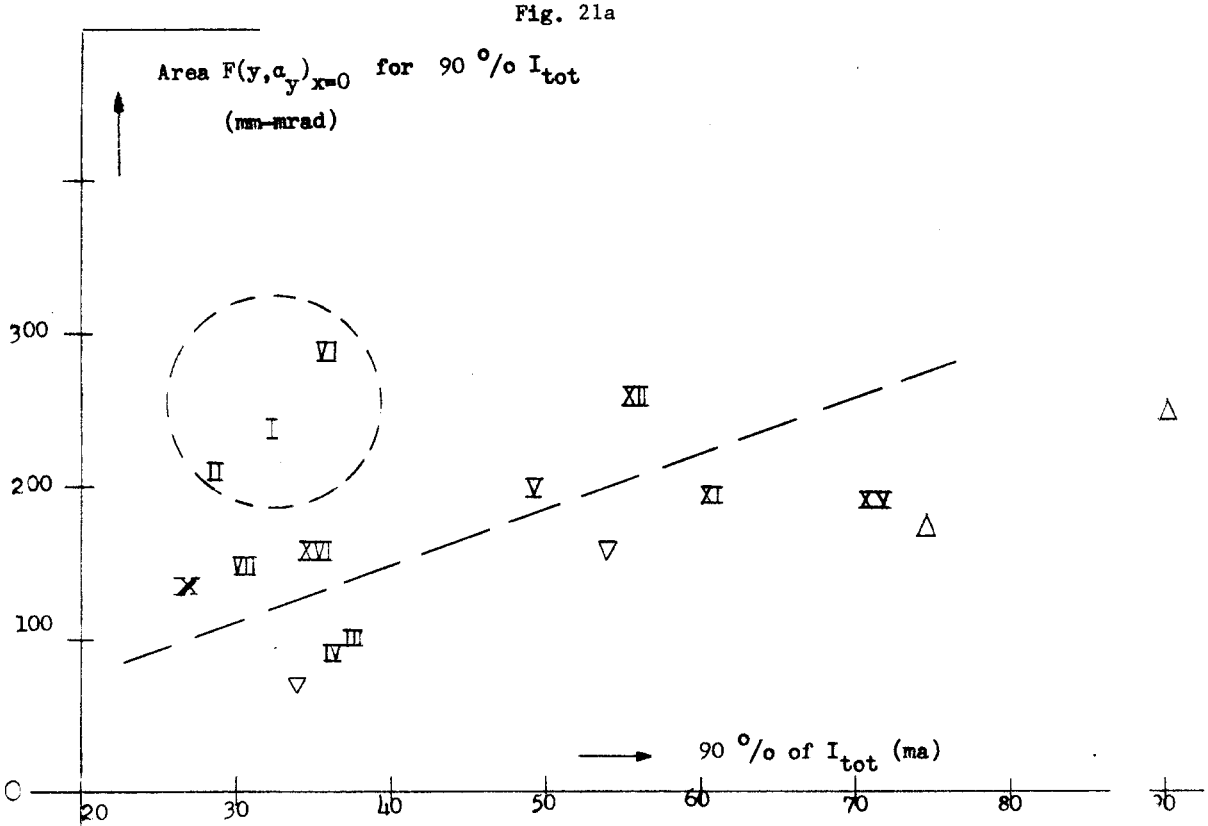

Fig. 21b